

**STRUCTURAL AND OPTOELECTRONIC
STUDIES OF Er³⁺/Yb³⁺ CO-DOPED
SrBi₂Nb₂O₉ FERROELECTRIC CERAMIC**

A Thesis Submitted

in Partial Fulfillment of the Requirements for the

Degree of

MASTER OF SCIENCE

in

PHYSICS

by

ABDUL BASITH

(2K22/MSCPHY/01)

SHOBHANGNA SINGH

(2K22/MSCPHY/36)

Under the supervision of

DR. RENUKA BOKOLIA



DEPARTMENT OF APPLIED PHYSICS

DELHI TECHNOLOGICAL UNIVERSITY

(Formerly Delhi College of Engineering)

**Shahbad Daultapur, Main Bawana Road, Delhi-110042,
India**

June, 2024

ACKNOWLEDGMENT

We express our sincere thanks and respect to everyone who helped us finish our dissertation project report successfully. This valuable learning experience would not have been possible without the help, direction, and inspiration of many people and institutions. First and foremost, we extend our deepest thanks to our project supervisor, Dr. Renuka Bokolia, Assistant professor, for providing us with this wonderful opportunity to work on the “Structural and Optoelectronic Studies of Er³⁺/Yb³⁺ co-doped SrBi₂Nb₂O₉ ferroelectric Ceramic”. Their expertise, patience, and constructive feedback have been instrumental in shaping this work.

We are deeply thankful to Ms. Ankita Banwal and Mrs. Megha Narwan for fostering a positive work environment and sharing their valuable research experience. Their insightful comments, suggestions, and discussions, have enriched my understanding of the subject matter. We're very thankful for the willingness to share knowledge, answer our questions, and engage in discussions greatly enriched our learning experience and enhanced the overall quality of this project.

We express our gratitude to our family for their constant support, love, and patience during our studies. Their confidence in our skills has served as an ongoing source of inspiration.

We are appreciative of our friends and colleagues' encouragement, support, and companionship throughout this academic adventure. Their camaraderie has helped to make both challenges and achievements more joyful.

Finally, we would like to acknowledge the participants and individuals who contributed to this research, whether through participation in interviews, providing access to resources, or helping in various forms. Your contributions are deeply appreciated. In conclusion, we are truly grateful to everyone who has contributed to the completion of our project report.

Abdul Basith

(2K22/MSCPHY/01)

Shobhangna Singh

(2K22/MSCPHY/36)



DELHI TECHNOLOGICAL UNIVERSITY
(Formerly Delhi College of Engineering)
Shahbad Daultpur, Main Bawana Road, Delhi-42

CANDIDATE'S DECLARATION

We, Abdul Basith(2K22/MSCPHY/01) and Shobhangna Singh (2K22/MSCPHY/36) hereby certify that the work which is presented in Major Project-II/Research work thesis entitled “Structural and Optoelectronic Studies of $\text{Er}^{3+}/\text{Yb}^{3+}$ co-doped $\text{SrBi}_2\text{Nb}_2\text{O}_9$ Ferroelectric Ceramic” in fulfillment of the requirements for the award of the Degree of Masters of Science in Physics, submitted in the department of Applied Physics, Delhi Technological University is an authentic record of our work carried out during the period from July 2023 to June 2024 under the supervision of Dr. Renuka Bokolia.

The matter presented in the thesis has not been submitted by us for the award of any other degree of this or any other Institute. The work has been accepted in a peer-reviewed Scopus-indexed conference with the following details:

- **Title of paper:** Structural, photoluminescence, and ferroelectric behaviour of $\text{Er}^{3+}/\text{Yb}^{3+}$ co-doped $\text{SrBi}_2\text{Nb}_2\text{O}_9$ ferroelectric ceramic for multifunctional devices
- **Author Names (in sequence as per research paper):** Shobhangna Singh, Abdul Basith, Ankita Banwal, Megha Narwan, Renuka Bokolia
- **Name of conference/Journal:** International Conference on Atomic, Molecular, Material, Nano, and Optical Physics with Applications (ICAMNOP-2023)
- **Conference Date with venue (if applicable):** 21st of December,2023
- **Have you registered for the conference? (Yes/No):** Yes
- **Status of paper (Accepted/published/communicated):** Accepted
- **Date of paper communication:** 01st of April,2024

- **Date of paper acceptance:** 01st of June,2024

Place: Delhi

Abdul Basith (2K22/MSCPHY/01)

Date:

Shobhangna Singh (2K22/MSCPHY/36)

This is to certify that the student has incorporated all the corrections suggested by the examiners in the thesis and that the statement made by the candidate is correct to the best of our knowledge.

Place: Delhi


Dr. Renuka Bokolia

Date:

(Assistant Professor)



DELHI TECHNOLOGICAL UNIVERSITY
(Formerly Delhi College of Engineering)
Shahbad Daultpur, Main Bawana Road, Delhi-42

CERTIFICATE BY THE SUPERVISOR

Certified that Abdul Basith (2K22/MSCPHY/01) and Shobhangna Singh (2K22/MSCPHY/36) have carried out their search work presented in this thesis entitled “Structural and Optoelectronic Studies of $\text{Er}^{3+}/\text{Yb}^{3+}$ co-doped $\text{SrBi}_2\text{Nb}_2\text{O}_9$ Ferroelectric Ceramic” for the award of Mater of Science in Physics from Department of Applied Physics, Delhi Technological University, Delhi, under my supervision. The thesis embodies the results of the original work, and studies are carried out by the students. The contents of the thesis do not form the basis for the award of any other degree to the candidate or anybody else from this or any other University/Institution. The work has been communicated in peer-reviewed Scopus-indexed conferences with the following details:

Title of paper: Structural, photoluminescence, and ferroelectric behaviour of $\text{Er}^{3+}/\text{Yb}^{3+}$ co-doped $\text{SrBi}_2\text{Nb}_2\text{O}_9$ ferroelectric ceramic for multifunctional devices

Author Names (in sequence as per research paper): Shobhangna Singh, Abdul Basith, Ankita Banwal, Megha Narwan, Renuka Bokolia

Name of conference/Journal: International Conference on Atomic, Molecular, Material, Nano, and Optical Physics with Applications (ICAMNOP-2023)

Conference Date with the venue (if applicable): 21st of December, 2023

Have you registered for the conference? (Yes/No): Yes

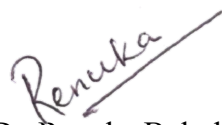
Status of paper (Accepted/published/communicated): Accepted

Date of paper communication: 01st of April, 2024

Date of paper acceptance: 01st of June, 2024

Place: Delhi

Date:


(Dr. Renuka Bokolia)
(Assistant Professor)

STRUCTURAL AND OPTOELECTRONIC STUDIES OF Er³⁺/Yb³⁺ CO-DOPED SrBi₂Nb₂O₉ FERROELECTRIC CERAMIC

Abdul Basith, Shobhangna Singh

ABSTRACT

A series of SrBi_{2-x-y}Nb₂Er_xYb_yO₉ ferroelectric ceramics (x= 0.03, y= 0.01, 0.03,0.06, 0.09, and 0.12) has been prepared by the solid-state reaction method. The precursors SrCO₃, Bi₂O₃, and Nb₂O₅ were used for undoped SrBi₂Nb₂O₉ (SBN) while Er₂O₃, and Yb₂O₃ were used as dopants. Calcination of powder at 950°C for 3 hours and then pellets were sintered for 3 hours at 1050°C. The formation of pure phase SBN has been confirmed by XRD spectra corresponding to orthorhombic geometry having phase group A21am. The highest intensity plane was observed at (115) for all SBN compositions, conceding the bismuth layered structure with n = 2. Evaluation of lattice parameters from XRD shows the increase in orthorhombic distortion i.e., b/a value as the concentration of Yb³⁺ increases. The lattice parameters and unit cell volume increase as the content of Yb³⁺ rises. SEM study reveals the randomly oriented plate-like structure of SBN. Their average particle sizes range from 1.12µm to 2.23µm to the concentrations x=0.03 and y=0.03. After a further rise in Yb³⁺ concentration, the average particle size decreases as the internal structure of the lattice is disrupted. The FTIR characteristic bands are found at wavenumber 540cm⁻¹, 602cm⁻¹, and 812cm⁻¹. In PL spectra, two green emission bands (524nm and 549nm) and one weak red band (660 nm) are acquired using a 488nm excitation wavelength. The highest PL intensity is found at x=0.03, y=0.03 after this concentration the intensity degrades because of the concentration quenching effect. The excitation spectra are obtained at the emission wavelength of 549nm with maximum excitation obtained at 488nm. The UCL spectra excited by 980nm laser, show two UCL bands at 524nm and 549nm in the green region and a single red band at 660nm. The green band dominates for initial concentration up to x = 0.03, y = 0.03 after which red emission dominates as the concentration of Yb³⁺ increases. The findings suggest the tunability of green light into red light of Yb³⁺ doped Er³⁺ - SBN ferroelectric ceramic. Pump power analysis shows that the two photons contribute to green and red UC emissions. The time decay analysis of SBN composition showed that the average decay time of Er³⁺ is 70µs and that of Yb³⁺ is 37µs. The diffuse reflectance spectra revealed the band gaps of the ceramic samples ranging from values 2.7eV to 3.1eV.

TABLE OF CONTENTS

1. INTRODUCTION

- 1.1 WHAT IS FERROELECTRIC CERAMIC?
- 1.2 TYPES OF FERROELECTRIC CERAMICS
- 1.3 WHY FERROELECTRIC MATERIAL AS HOST MATERIAL
- 1.4 APPLICATION OF FERROELECTRIC MATERIALS
- 1.5 ADVANTAGES OF FERROELECTRIC CERAMICS
- 1.6 LIMITATIONS OF FERROELECTRIC CERAMICS
- 1.7 ADDRESSING THE LIMITATIONS
- 1.8 LUMINESCENCE
- 1.9 LUMINESCENCE BASED ON TIME DECAY
- 1.10 PHOTOLUMINESCENCE
- 1.11 TYPES OF PHOTOLUMINESCENCE
- 1.12 BASIC REQUIREMENTS FOR UCL
- 1.13 UPCONVERSION MECHANISM
- 1.14 IMPORTANCE OF RARE-EARTH DOPANTS

2. LITERATURE REVIEW

- 2.1 WHY SBN AS HOST MATERIAL
- 2.2 CRYSTAL STRUCTURE OF SBN
- 2.3 WHY Er^{3+} AND Yb^{3+} AS RARE EARTH DOPANTS?

3. SYNTHESIS

- 3.1 SOLID-STATE REACTION METHOD
- 3.2 SAMPLE PREPARATION USING SOLID-STATE REACTION METHOD

4. CHARACTERIZATION TECHNIQUES

- 4.1 STRUCTURAL CHARACTERIZATION-XRD
- 4.2 STRUCTURAL CHARACTERIZATION-SEM
- 4.3 CHEMICAL CHARACTERIZATION-FTIR
- 4.4 OPTICAL CHARACTERIZATION-PL, UCL
- 4.5 UV-VISIBLE SPECTROSCOPY

5. EXPERIMENTAL RESULTS

- 5.1 X-RAY DIFFRACTION(XRD)
- 5.2 SCANNING ELECTRON MICROSCOPE (SEM)
- 5.3 FOURIER TRANSFORM INFRARED (FTIR) SPECTROSCOPY
- 5.4 PHOTOLUMINESCENCE (PL)
- 5.5 UP CONVERSION LUMINESCENCE (UCL)
- 5.6 INFLUENCE OF PUMP POWER ON UCL
- 5.7 TIME DECAY ANALYSIS
- 5.8 UV-VISIBLE SPECTROSCOPY

6. RESULTS AND CONCLUSIONS

7. REFERENCES

8. APPENDICES

LIST OF TABLES

Table 1: Chemical composition and their respective sample code for the series of $\text{SrBi}_{2-x-y}\text{Nb}_2\text{Er}_x\text{Yb}_y\text{O}_9$ (SBN)

Table 2: Lattice parameters for all compositions of SBN ferroelectric ceramics.

Table 3: Fluorescence Time decay values for the series of SBN ferroelectric ceramic.

LIST OF FIGURES

Fig.1-Types of Luminescence

Fig.2-Fluorescence and phosphorescence

Fig.3-Photoluminescence

Fig.4-Up Conversion mechanism

Fig.5-Steps to synthesize SBN

Fig.6-Bragg's law

Fig.7-Bruker D8 diffractometer

Fig.8-Scanning Electron Microscopy (SEM)

Fig.9-PerkinElmer Spectrum FTIR spectrometer

Fig.10-Up-conversion/ down-conversion Fluorescence spectroscopy

Fig.11-UV-Visible spectroscopy

Fig.12-(a)XRD spectra for the series of SBN ferroelectric ceramics. (b)Shifting of the peak for various dopant concentrations.

Fig.13-SEM analysis of a series of SBN ferroelectric ceramics.

Fig.14-SEM histograms of series of SBN ferroelectric ceramic.

Fig.15-(a) FTIR spectra for the series of SBN ferroelectric ceramic, (b) FTIR band as the function of dopant concentration for wavenumber 602cm^{-1} , (c) FTIR band as the function of dopant concentration for wavenumber 812cm^{-1}

Fig.16-(a) Excitation spectra, (b) Emission spectra for the series of SBN ferroelectric ceramic

Fig.17-UCL spectra of the series of SBN ferroelectric ceramics.

Fig.18-CIE plot of the series of SBN ferroelectric ceramics except SBNE0Y0

Fig.19-Energy transfer pathways between Yb^{3+} - Er^{3+} ions under 980 nm excitation

Fig.20- Enhancement in the green and red emission band intensities as the function of Yb^{3+} content.

Fig.21-(a) Dexter plot of $\log(I/X)$ versus $\log(X)$ for 549 nm (b) Dexter plot of $\log(I/X)$ versus $\log(X)$ for 660 nm

Fig.22-(a) Pump power dependency on UCL intensity of SBNE3Y3 ferroelectric ceramic (b) Log plot of pump power and UC intensity

Fig.23-Pump power dependency on UCL intensity of SBNE3Y12 ferroelectric ceramic.

Fig.24-Time decay plots of all compositions of SBN ferroelectric ceramic at 549nm

Fig.25-Time decay plots of all compositions of SBN ferroelectric ceramic at 660nm

Fig.26- Variation of decay lifetime with Yb^{3+} concentration

Fig.27-UV-visible spectra of all compositions of SBN ferroelectric ceramic.

Fig.28- Tauc Plots of all compositions of SBN ferroelectric ceramic represented with their respective bandgaps.

LIST OF SYMBOLS, ABBREVIATIONS, AND NOMENCLATURE

SBN: Strontium Bismuth Niobate or $\text{SrBi}_{2-x-y}\text{Nb}_2\text{Er}_x\text{Yb}_y\text{O}_9$

RE: Rare Earth

Er^{3+} : Erbium

Yb^{3+} : Ytterbium

NVRAM: Non-volatile Random-access memory

BLSF: Bismuth-layered structured ferroelectrics

Fig.: Figure

C.No.: Co-ordination number

XRD: X-Ray Diffraction

SEM: Scanning Electron Microscope

FTIR: Fourier Transform Infrared

PL: Photoluminescence

UCL: Upconversion luminescence

NIR: Near Infrared Radiation

GSA: Ground state absorption

ESA: Excited state absorption

ET: Energy transfer

MPR: Multi-phonon relaxation

CR: Cross relaxation

UV-Vis: Ultraviolet-Visible

DRS: Diffuse Reflectance Spectroscopy

CHAPTER-1: INTRODUCTION

1.1 WHAT IS FERROELECTRIC CERAMIC?

Ferroelectric ceramics, an intriguing class of materials offers a unique combination of structural and electrical characteristics. Because they have potential applications in a wide range of technological domains, they have become a cornerstone for research across multiple fields [1]. Core Properties:

- ✓ **Spontaneous Polarization:** The defining characteristic of a ferroelectric ceramic is its spontaneous electric polarization. This means that when not subjected to any external electric field, the material exhibits a permanent electric dipole moment within its crystal structure. This arises from the displacement of positive and negative ions within the unit cell of the material.
- ✓ **Domain Structure:** The polarised areas, often referred to as ferroelectric domains, are usually randomly orientated in bulk ferroelectric ceramics. Nonetheless, the alignment of these domains may be affected by an external electric field, changing the material's total polarization.
- ✓ **Hysteresis Loop:** A ferroelectric ceramic exhibits a characteristic hysteresis loop in the presence of an alternating electric field. The relationship between the electric field subjected and the degree of polarisation generated within the material is illustrated by this loop. The energy lost throughout the cycle is represented by the region that the loop encloses.

1.2 TYPES OF FERROELECTRIC CERAMICS

- ✓ **Perovskites:** This is a widely studied family of ferroelectric ceramics with a general formula ABO_3 , where A and B are cations (positively charged ions) and O represents oxygen anions. Examples include lead zirconate titanate (PZT), Strontium Bismuth Niobate (SBN), and barium titanate ($BaTiO_3$).
- ✓ **Non-Perovskites:** Besides perovskites, other materials like lithium niobate ($LiNbO_3$) and sodium niobate ($NaNbO_3$) also exhibit ferroelectric behavior.

1.3 WHY FERROELECTRIC MATERIAL AS HOST MATERIAL?

Materials that exhibit spontaneous polarisation, also known as remanent polarisation, and reversible behavior in the presence of an electric field, are known as ferroelectric materials. Due to the unique characteristics, they possess, ferroelectric materials have attracted a lot of interest. These include significant dielectric constant, high fatigue resistance, large Curie temperature, and piezoelectric effects. Ferroelectric materials often exhibit piezoelectric properties, which means they can produce an electric charge in response to mechanical stress. They also exhibit nonlinear optical properties, making them useful in applications where nonlinear effects are exploited, such as in frequency conversion processes. Up-conversion luminescence involves nonlinear

processes, and the unique optical properties of ferroelectric materials may contribute to enhancing the efficiency of these processes. The electronic structure of ferroelectric materials can be tuned, allowing for control over the energy bandgap. Ferroelectric materials are often stable and durable, with good thermal and chemical resistance. Bismuth-layered structured ferroelectrics (BLSF) and ferroelectric perovskites have been instances of multifunctional oxide materials that have been explored as potential hosts for the integration of luminescent and functional piezoelectric characteristics. Due to its (i) low phonon energy, (ii) capability for modifying the crystal structure using dopants, and (iii) ability to add optical functionality to their functional piezoelectric capabilities, rare earth-doped ferroelectric host materials continue to be of interest. In addition to investigating whether luminescent properties could react to external stimuli including electric fields, mechanical strain, and temperature, their intriguing coupling effects are of relevance for the development of smart materials.

1.4 APPLICATIONS OF FERROELECTRIC MATERIAL

Ferroelectric ceramics are a very interesting class of materials that exhibit a unique interaction between structural and electrical properties. They're a fundamental component of study in many scientific fields because of their intrinsic spontaneous polarization and the ability to control this state using electric fields [1,2]. The main uses of ferroelectric ceramics that are propelling progress in a variety of fields of study are:

- ✓ Ferroelectric ceramics' piezoelectric nature contributes to one of their most widely used applications. They can transform mechanical stress or pressure into an electrical voltage due to this property. On the other hand, when an electric field is applied, the material may physically alter. Given this bidirectional nature, ferroelectric ceramics are beneficial for:
 - Sensors: They're appropriate to be utilized as pressure sensors in medical ultrasound imaging systems, automobile airbags, and microphones given their capacity to detect variations in pressure. Ferroelectric ceramics are also used by accelerometers in motion detectors, vibration sensors, and force sensors in robotics and touchscreens to detect motion and force accurately.
 - Actuators: The converse piezoelectric effect enables the creation of highly precise actuators. If an electric field is applied, these actuators can alter their shape, enabling precise micro-movements. Inkjet printer heads, car fuel injectors, and microfluidic devices for small-scale fluid manipulation are a few examples of applications.
- ✓ Many ferroelectric ceramics possess an exceptionally high permittivity. Thus, for a given voltage, they can store a significant amount of electrical charge. Ferroelectric ceramics' high permittivity makes it feasible to generate Multilayer Ceramic Capacitors (MLCs), which are crucial parts of electronic systems that filter electrical noise, smooth signals, and stabilize power supply. They're an

essential component in modern electronics due to their small size and effective operation.

- ✓ An additionally noteworthy property of ferroelectric ceramics is the electrostrictive effect. These materials suffer a slight form change in the presence of an electric field. The electrostrictive effect causes minute yet controllable shape changes, which are used in tunable filters for telecommunication systems and microlenses for optical devices. The transmission of light and signals may be finely regulated due to these little changes [1-4].

- ✓ Ferroelectric materials' characteristic hysteresis loop opens the door to innovative memory solutions. This non-volatile memory system takes into account ferroelectric materials' switchable polarization state. As compared to conventional volatile RAM, the two polarization states offer a significant benefit in data retention as they represent binary data (0 or 1) that persists even after power is turned off.

- ✓ The potential of ferroelectric ceramics is being deeply investigated in several fresh areas of research:
 - Energy Harvesting: Energy harvesting applications could benefit from ferroelectrics' potential to transform mechanical vibrations into electrical currents. This could result in the development of microdevices and sensors which operate on their power.

 - Spintronics: Devices utilizing ferroelectric ceramics along with magnetic materials can pave the way for spintronics. These devices exploit the spin of electrons for functionalities beyond conventional charge-based electronics, potentially leading to breakthroughs in data storage and processing.

1.5 ADVANTAGES OF FERROELECTRIC CERAMICS

Ferroelectric ceramics are the backbone of billion-dollar industries from high dielectric capacitors to positive temperature coefficient devices and electro-optic valves because they have great features such as high dielectric permittivity, outstanding piezoelectric response, and swappable macroscopic polarization. The following are the advantages of ferroelectric ceramics:

- ✓ Piezoelectricity: They generate pressure or tension into a measurable voltage, making it suitable for a wide range of sensors. When it comes to sensing and changing physical events into electricity, ferroelectrics thrive. They exist in a wide range of devices, including accelerometers in motion detectors, transducers for ultrasound imaging, and pressure sensors in airbags and microphones. Also, this property is used for actuators due to the converse piezoelectric effect, they can change their form and function as actuators when an electric field is applied. This precise control over movement has applications in inkjet printer heads, vehicle fuel

injectors, and microfluidic devices, enabling controlled manipulation at the micro level [4-6].

- ✓ Many ferroelectric ceramics offer a very high permittivity, which means they can store a lot of electrical charge in a small area. This characteristic is essential to the electronic component's downsizing.
- ✓ They are the foundation of Multilayer Ceramic Capacitors (MLCs) due to their high permittivity. These fundamental parts of electronics are crucial for stabilizing power supply, smoothing signals, and filtering noise. Among the main benefits of contemporary miniaturized electronics are their small size and effective performance
- ✓ Memory storage: Ferroelectric Random-Access Memory (FRAM) is achievable given the special hysteresis loop of ferroelectric materials. Unlike traditional RAM, this non-volatile memory technology has several advantages. For applications like industrial control units and embedded systems, the material's switchable polarization state ensures dependable data retention by representing data (0 or 1) even in the event of power failure [5].
- ✓ Material versatility: Ferroelectric ceramics can be made from a wide variety of materials, each with distinctive features. This optimizes performance by enabling researchers and engineers to customize the choice of materials for certain applications.
- ✓ Processing Potential: Cost-effective and scalable manufacturing is made possible by the fact that many ferroelectric ceramics can be processed using conventional techniques like sintering.

1.6 LIMITATIONS OF FERROELECTRIC CERAMICS

Ferroelectric ceramics give an unexpected variety of advantages; however, they are not without disadvantages. To optimize material selection and application design, researchers and engineers need a thorough understanding of these disadvantages. Here's a closer look at the major challenges that ferroelectric ceramics deal with:

- ✓ Brittleness: Under mechanical stress or impact, many ferroelectric ceramics can break due to their intrinsic brittleness. This may restrict its use in scenarios when strong mechanical qualities are necessary.
- ✓ Fatigue: When ferroelectric materials are repeatedly subjected to mechanical stress or electric field cycling, their performance may gradually deteriorate. Fatigue is a problem that can result in decreased performance and device malfunction.
- ✓ High-Temperature Sensitivity: Certain ferroelectric ceramics have characteristics that are extremely susceptible to changes in temperature. This could limit their range of operation in settings with large temperature fluctuations.

- ✓ **Lead Content:** Principal Content Lead-based ferroelectric ceramics, like lead zirconate titanate (PZT), have been utilized traditionally and perform well. However, the search for lead-free substitutes has been fueled by worries about lead's effects on the environment and human health.
- ✓ **Sintering Requirements:** Ferroelectric ceramics sometimes require high sintering temperatures, which can be energy-intensive and restrict the kinds of substrates on which they can be placed. Integration with some electronic components may be hampered as a result.
- ✓ **High Coercive Field:** In certain ferroelectric ceramics, a high coercive field the electric field intensity necessary to change the polarization state may be necessary. This may result in higher power usage and restricted functionality of the gadget.
- ✓ **Leakage Current:** Certain ferroelectric materials can experience leakage current, which is a little current flow even when not subjected to an electric field. This may result in energy loss and might impair the functionality of the gadget [5-7].

1.7 ADDRESSING THE LIMITATIONS

Scholars are currently active in efforts to surmount these constraints:

- ✓ **Material Development:** The goal is to create ferroelectric ceramics devoid of lead that have better characteristics, such as lower coercive fields, greater operating temperatures, and lower leakage currents.
- ✓ **Composite Materials:** Ferroelectric ceramics can be combined with other materials to create composite materials that have the potential to improve mechanical characteristics and reduce brittleness.
- ✓ **Thin Film Technologies:** New developments in thin film deposition methods enable integration with a larger variety of substrates by permitting the formation of 56xferroelectric films at lower temperatures.

1.8 LUMINESCENCE

The term “luminescence” was introduced by Wiedemann in the year 1888. It should not be confused with incandescence, as these two are completely different. Incandescence is the process where heat energy converts into light energy. For example, when an iron bar is heated at a high temperature and the temperature rises it starts glowing from red to white [6-7]. Whereas, Luminescence refers to the emission of light by a substance that is not due to heat. It’s a cold body radiation emitted in the form of photons without any externally applied heat. Instead of heat, other external

exciters such as photons, chemical reactions, subatomic motions, electrons, stress, etc. are used. Luminescence includes the visible region (380nm-780nm), and ultraviolet and infrared region of the emission spectrum. The human eye is active in the range of 380nm-780nm and is most responsive around 555nm. So, commercial phosphors are used to emit light in this band of wavelengths.

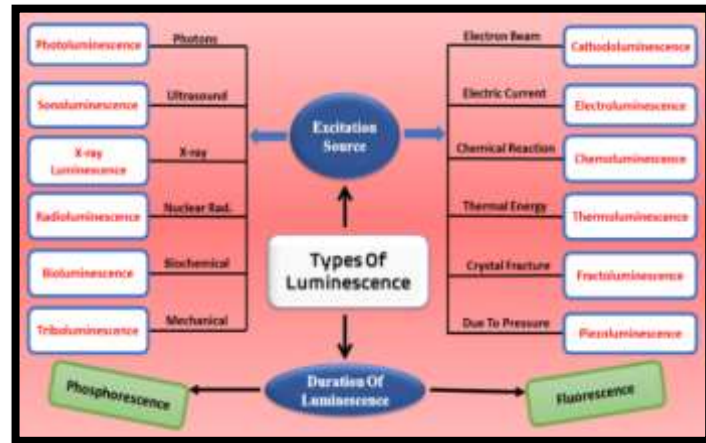


Fig.1-Types of Luminescence

1.9 LUMINESCENCE BASED ON TIME DECAY

Luminescence is classified based on its lifetime or luminescent duration. Luminescence when the lifetime is shorter than 10^{-8} s is called fluorescence, while longer luminescence is known as phosphorescence.

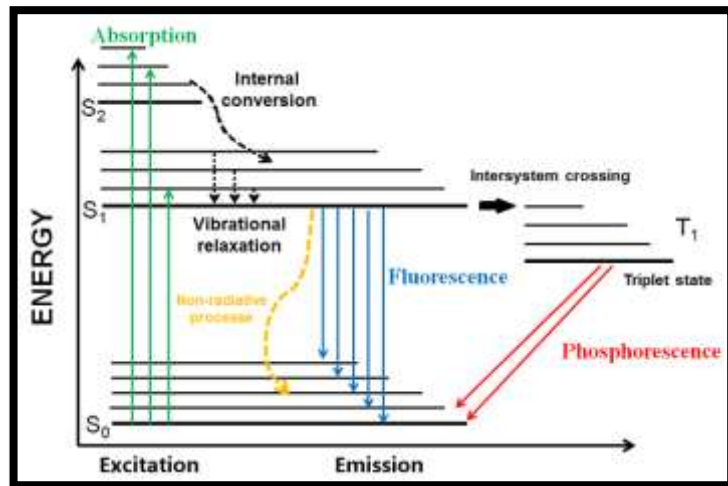


Fig.2-Fluorescence and phosphorescence

- ✓ **Fluorescence:** Fluorescence is a phenomenon where a substance absorbs light at a specific wavelength and promptly re-emits light or photons at a longer wavelength i.e., low energy. This process occurs due to the temporary excitation of electrons to higher energy levels, followed by their rapid return to lower energy levels. In quantum theory, when a substance emits light during fluorescence, the transitions

occur from a specific excited state called the singlet state. In this state, the electron's spin direction remains the same. The emitted light, known as fluorescence, usually occurs within nanoseconds after the absorption of the excitation light.

- ✓ Phosphorescence: Process in which a substance absorbs and stores energy, typically from light, and then emits that energy as light over an extended period. Transitions from the triplet excited state are not allowed according to the selection rules in quantum theory. As a result, the electron in the triplet state takes a relatively long time until its spin flips back.

1.10 PHOTOLUMINESCENCE

When a molecule absorbs a photon, one of its electrons grows excited and jumps to a higher energy electronic excited state. The high-energy electron eventually returns to its less excited state, resulting in photoluminescence (PL), an optical phenomenon characterized by the emission of two or more photons of a longer wavelength, i.e., low energy in the visible region. It is a process where light is emitted from any matter upon excitation by photons. The method includes various routes to re-radiate the photons, such as light emission, energy transfer, and absorption. Among the mentioned routes, absorption occurs between ground and excited energy levels, while energy transfer occurs only between excited energy levels. Luminescence is only observed when there is absorption of photons. Photon absorption either occurs at the luminescent center or at any other place in the host lattice. If absorption takes place at the luminescent center, there is direct emission. But if it is at any other site in the host lattice, energy transfer occurs to the luminescent center so that emission can occur [5-10]. At last, Photoluminescence is the emission of light which is caused by the irradiation of material with other light.

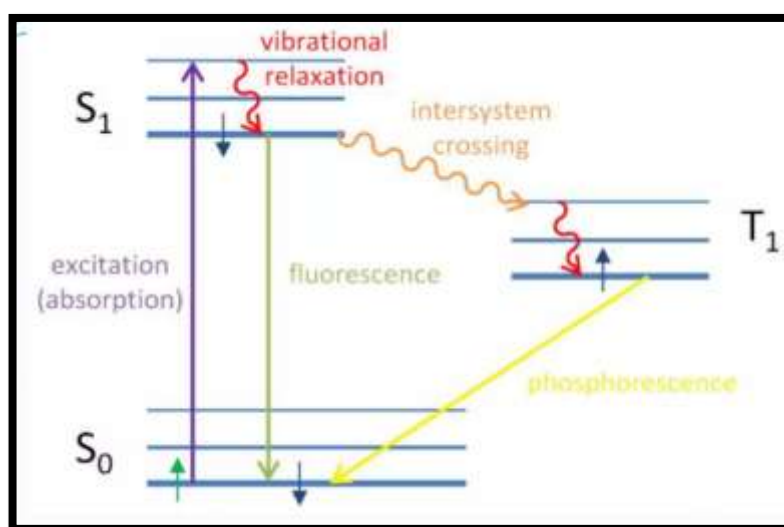


Fig.3-Photoluminescence

1.11 TYPES OF PHOTOLUMINESCENCE

Types of photoluminescence based on the energy of the photon emitted during photoluminescence two types of photoluminescence are:

- ✓ Down-conversion luminescence: Down-conversion luminescence is the process where materials absorb higher-energy photons, and the emitted photons have lower energy. It's observed in many types of phosphors and fluorescent materials. Here a material absorbs photons with higher energy, typically in the ultraviolet or visible range, and then re-emits photons with lower energy, generally in the visible or infrared range. This shift to lower energy is a result of electronic transitions within the material [9,10].
- ✓ Upconversion luminescence (UCL): In contrast, upconversion leads to the conversion of lower-energy photons into higher-energy photons. This process is often achieved through the use of rare-earth ions in certain materials. It's interesting because it allows the harnessing of low-energy light, such as infrared radiation, and converting it into higher-energy visible or ultraviolet light. In upconversion, the material absorbs two or more lower-energy photons and combines their energy to emit a single photon with high energy.

1.12 BASIC REQUIREMENTS FOR UCL

- ✓ Host selection: Generally, the host materials are oxides, nitrides and oxynitrides, sulfides, selenides, halides, or silicates of zinc, cadmium, manganese, aluminium, silicon, or various rare-earth metals. The two types of lead-free piezoelectric materials are inorganic and organic materials. The selected host should have small phonon energy, high thermal and chemical stability, and low toxicity i.e., lead-free.
- ✓ Choice of dopants: The choice of dopants for up-conversion luminescence is a critical factor in designing materials that efficiently convert lower-energy photons into higher-energy photons. Various dopant ions, particularly rare-earth ions are excellent dopants for up-conversion because of their high luminescence efficiency and cost-effective synthesis. The specific choice of dopants depends on the desired wavelength range for up-conversion, the application requirements, and the efficiency of the up-conversion process. Often, combinations of dopants are utilized to achieve optimal performance, leveraging their complementary absorption and emission characteristics [11,12]. Rare earth ions are very common components in many up-conversion phosphors due to their well-defined energy states.
- ✓ Amount of dopants in host material: The concentration of doping levels should be optimized. Too high concentrations may lead to quenching effects, where interactions between dopant ions result in non-radiative energy transfer processes. This can reduce the overall up-conversion efficiency. It should be minimal so that

the concentration quenching can be avoided. Emission intensity decreases if the concentration of the dopant is too high.

1.13 UPCONVERSION MECHANISM

Upconversion involves basic processes: ground state absorption (GSA), energy transfer (ET), excited state absorption (ESA), multi-phonon relaxation (MPR), and radiative emission.

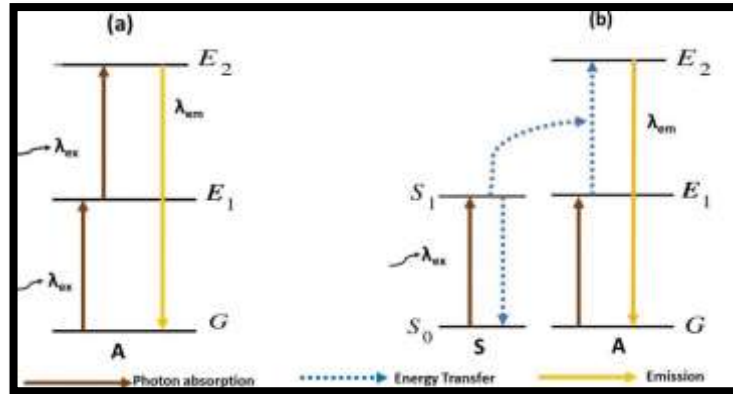


Fig.4- Up Conversion mechanism

The photon incident is absorbed by the ground state energy level (G). Through this energy absorption, electrons reach an excited energy level (E_1). GSA is a simple process where the activator absorbs energy. If there is a simple radiative emission only after GSA, the luminescence will be down conversion, i.e., a lower energy photon will be emitted. But for upconversion, excited state absorption takes place, meaning another photon is absorbed by the excited state to further excite the electrons to higher energy levels (E_2) as shown in Fig. 4(a). The radiative emission from energy level E_2 will result in emission photons having greater energy than the incident photons. The mechanism of upconversion is not as simple as it seems, as many non-radiative emissions are involved, which seems to cause a loss of energy. This non-radiative emission includes multi-phonon relaxation. When the electrons are excited to higher energy levels, they often reach short-lived energy levels. These energy levels are not stable enough to cause a radiative de-excitation directly to the ground state, which is crucial to observe an upconversion luminescence. So, these higher excited energy levels reach much more stable excited states by MPR. It is the de-excitation of electrons in the host lattice by losing energy in the form of phonons or lattice vibrations[13].

There is another mechanism of upconversion when sequential absorption of incident photons take place, intending two or more incident photons are absorbed simultaneously. In this case, a sensitizer ion is used, which helps in populating the metastable state of the activator ion as shown in Fig. 4(b). A sensitizer ion absorbs a photon, then electrons reach an excited state, and it relaxes and reaches the ground state by giving away the energy absorbed to the activator ion. This helps in the overpopulation of metastable state (E_2) in activator ion, which radiatively de-excites and releases photons of higher energy (anti-stokes shift). This energy transfer acts as

a catalyst to the upconversion process and also increases the intensity of luminescence observed. The most commonly used sensitizer is ytterbium to activator ion erbium[14]. It should be noted that GSA and ESA only occur when incident photons have energy comparable to the energy difference between G , E_1 , and E_2 , and energy transfer takes place when the energy difference of S_0 and S_1 of the sensitizer ion should be comparable to the energy difference between E_1 and E_2 .

1.14 IMPORTANCE OF RARE-EARTH DOPANTS

Rare earth dopants are crucial for the modification and enhancement of the properties of materials, especially in solid-state physics and materials science. The term "rare earth" refers to a group of elements in the periodic table, including lanthanides such as neodymium (Nd), europium (Eu), gadolinium (Gd), and others. Rare earth elements have distinctive electronic configurations due to the filling of 4f orbitals, providing them with unique magnetic and optical properties. This uniqueness makes them highly desirable for introducing tailored characteristics into host materials. Rare earth dopants are frequently utilized in semiconductor technologies. For example, neodymium-doped yttrium aluminium garnet is widely employed as a laser material in solid-state lasers, owing to its unique optical properties. Some rare earth elements, such as gadolinium and dysprosium, exhibit strong magnetic properties. Doping magnetic materials with these elements can enhance or introduce magnetic functionalities, making them useful in applications like magnetic data storage. Rare earth dopants are renowned for their distinct optical characteristics. Europium, for instance, is known for its ability to emit red fluorescence when incorporated into phosphors, making it valuable in display technologies and lighting [15]. Rare earth elements are commonly used in the production of phosphors for various devices, including cathode-ray tubes (CRTs), light-emitting diodes (LEDs), and fluorescent lamps, due to their ability to emit specific colors of light. While rare earth dopants offer unique properties, there are concerns about the environmental impact of mining and processing rare earth elements. Efforts are underway to develop sustainable practices and alternative materials that reduce dependence on these elements.

CHAPTER-2: LITERATURE REVIEW

2.1 WHY SBN AS HOST MATERIAL?

Ferroelectric materials are materials that hold reversible and spontaneous polarization when subjected to an electric field. They are widely preferred in industries from high-dielectric capacitors to positive temperature coefficient devices. They hold excellent properties like high dielectric constant, significant fatigue resistance, large curie temperature, and piezoelectric effects making them desirable materials for various applications like non-volatile random-access memories (NVRAM), pyroelectric infrared detectors, large capacitance capacitors, and optical switches, etc[16-17]. When doped with rare earth ferroelectric materials are frequently utilized for luminescent host materials because they can be readily excited from near-infrared regions to higher energy levels using low-energy and affordable laser devices.

Our literature review reveals that the popularity of Bismuth's layered structure ferroelectric (BLSF) materials is rapidly rising because of their good chemical and heat stability, good radiative transitions, lower phonon energy, and high-temperature sensitivity. BLSFs are also lead-free ceramics thereby, being non-toxic and environment friendly. Also, for an effective UCL, materials need to possess lower phonon energy to avoid or reduce the MPR process and to prolong the lifetime of the excited state in the material. The BLSFs with $(\text{Bi}_2\text{O}_2)^{2+}(\text{A}_{n-1}\text{B}_n\text{O}_{3n+1})^{2-}$ as a chemical formula are considered to be good UC luminescent arrays due to their low phonon energy and chemical stability. The BLSFs ceramics are the member of Aurivillius family with the chemical formula: $(\text{Bi}_2\text{O}_2)^{2+}(\text{A}_{n-1}\text{B}_n\text{O}_{3n+1})^{2-}$, where A is mono-, di-, or trivalent element (or their combination) with coordination no. 12, say, Ba^{2+} , Ca^{2+} , La^{3+} , Sm^{3+} , Bi^{3+} , Sr^{2+} , etc., further B is a transition element suited to octahedral coordination possessing coordination no. 6 like Fe^{3+} , Nb^{5+} , Ti^{3+} , Ta^{5+} , W^{6+} , and Mo^{6+} , etc., and here, n shows the number of perovskite layers in between two bismuth oxide layers[15-17].

We considered SBN as our host material as it's a BLSF belonging to the Aurivillius family with n=2, which has come into limelight due to its less distortion, lower dielectric dissipation coefficient, and larger Curie temperature compared to other BLSFs. It's a lead-free ferroelectric ceramic therefore is ecofriendly and non-toxic. It also possesses a characteristic high curie temperature, T_c ($>900^\circ\text{C}$), large fatigue resistance, low dielectric loss, reasonable spontaneous polarization, and temperature-insensitive significant piezoelectric coefficient and is considered for high-temperature application. It has great application in NVRAM and fine frequency tolerance resonators [16-19].

2.2 CRYSTAL STRUCTURE OF SBN

A lead-free ferroelectric component of bismuth-layered structured ferroelectric (BLSF) ceramics with a complicated crystal structure is strontium bismuth niobate ($\text{SrBi}_2\text{Nb}_2\text{O}_9$, or SBN). With a 3-D network of corner-sharing octahedra, the cubic perovskite structure is the most prevalent structure for SBN that is currently understood. Oxygen ions (O^{2-}) usually form these octahedra. These octahedra are

arranged in a cubic pattern to form the unit cell of this SBN cubic perovskite structure. For the stable lattice, the ions of strontium, bismuth, and niobium are arranged as follows:

- ✓ Strontium Ions: The centers of the oxygen octahedra in the perovskite lattice, or the center of the unit cell, are occupied by strontium ions (Sr^{2+}), which are encircled by oxygen ions to form an octahedral coordination environment.
- ✓ Bismuth Ions: Usually found at the corners of the perovskite unit cell are bismuth ions (Bi^{3+}). Compared to strontium, bismuth has a higher ionic radius, which is accommodated by its location in the corners.
- ✓ Niobium Ions: Similar to strontium, niobium ions (Nb^{5+}) are found at the centers of oxygen octahedra. Niobium is essential for the ferroelectric characteristics of SBN. The niobium ion dislocation inside the octahedra is what causes the ferroelectric phase transition.
- ✓ Oxygen Ions: The strontium, bismuth, and niobium ions in the lattice are bound together by oxygen ions (O^{2-}), which also form the borders of the octahedra. The stabilization of the arrangement of crystals and subsequent development of the perovskite lattice is facilitated by the presence of oxygen ions [20].

2.3 WHY Er^{3+} AND Yb^{3+} AS RARE EARTH DOPANTS?

The literature review reveals that the carefully chosen and appropriate RE ion doping of BLSF materials gives enhanced electrical, optical, and sensing performances. Some RE ions like Er^{3+} , Eu^{3+} , Pr^{3+} , etc. are used as luminescence centers. Thus, by RE doping, also the luminescence of some ferroelectric materials can be enhanced. The majority of UC luminescent materials are compounds containing RE ions that can convert infrared radiation to visible light. Currently, RE ions with diverse energy levels of 4f configuration, like Ho^{3+} , Pr^{3+} , Tm^{3+} , Er^{3+} , etc. are used to achieve UCL. Er^{3+} doped ferroelectric ceramics have shown excellent optical and sensing in recent works. Here in the current work, we chose Er^{3+} as our dopant of its metastable energy level that can be easily and efficiently populated by a laser source operating at 980 nm and is convenient for UCL. Er^{3+} shows the most stable oxidation state as 3+; thus, it can substitute Bi^{3+} ions in the $\text{SrBi}_{2-x}\text{Nb}_2\text{Er}_x\text{O}_9$ ceramic. Due to its ladder-like energy structure, Er^{3+} possesses an extended excited state lifetime, and excellent UC photochromic modulation properties, therefore a preferred activator for the conversion of infrared radiation to visible UC fluorescence and laser. We methodically substitute Bi^{3+} ions with Er^{3+} ions, and characterization techniques like XRD, SEM, and FTIR are studied for structural analysis. The excitation wavelength of 980 nm has been used for UC emission studies, pump power dependence on UCL intensity is evaluated for optimum dopant content, and time decay analysis is done [15-20]. However, the luminescence efficiency of the single-doped system with Er^{3+} is very low, mainly resulting from the small cross-section absorption of the 4f-4f transition. So, Yb^{3+} , with a dual-energy structure, is used as an activator for sensitization. The addition of Yb^{3+} leads to an increase in the absorption cross-section near 980nm and thus UCL enhances

the co-doped RE ions through energy transfer. The CR phenomenon can occur between Yb^{3+} and Er^{3+} , which can also modulate the UCL color of the Er^{3+} ion. Recently, some literature reported that the physical properties and PL can be enhanced via $(\text{Er}, \text{Yb})^{3+}$ co-doping. Given the promising applications of SBN ceramics, $(\text{Er}, \text{Yb})^{3+}$ doped SBN ceramics are anticipated to produce such intensification outcomes [20-22].

CHAPTER-3: SYNTHESIS

3.1 SOLID-STATE REACTION METHOD

Reactions between solids are often referred to as solid-state reactions. It is defined classically as a reaction in which both reactants and the resulting products are solid. But in reality, a lot of reactions are categorized as solid-state reactions even if both the reactants are non-solid. For instance, the rusting of iron is a solid-state reaction where one of the reactants is solid and the other is gaseous. Solid-state reaction research has become ever more significant since this method is the sole way to create many polycrystalline solids [22]. Solid-solid reactions are complicated and need several parameters to be fulfilled. The structural analyses of the product include a variety of approaches as well.

The process of fine-grain metal combinations involves mixing different metal combinations, forming pellets, and subjecting them to controlled temperatures for a specific duration. Some metal compounds, such as metal oxides or salts, require extreme conditions like high temperatures and pressure for initiation of reactions in a molten flux or rapidly condensing vapor phase. In solid-state synthesis, it is crucial to describe the reaction rate. Solid-state processes must be completed thoroughly as options for purifying produced solids are limited. The reaction rate in solid-state reactions depends on various factors, like structural properties, shape, and surface area of the reactants, diffusion rate, and thermodynamic factors associated with nucleation and reaction. The precursors and preparation methods employed play a significant role in determining the chemical and physical properties of the final products [20-24].

Modern solid-state techniques extend beyond variations of the ceramic process. In solid-state metathesis, the metal compounds' reactions are initiated by energy such as a flame or a ball mill, and the heat generated during product and byproduct production promotes these reactions.

3.2 SAMPLE PREPARATION USING SOLID-STATE REACTION METHOD

The solid-state reaction method is a fundamental technique for the synthesis of materials with desired properties. In this process, solid reactants are intimately mixed, typically through grinding or ball milling, and then subjected to controlled heating. The method relies on the diffusion of atoms or ions through the solid state, allowing the formation of the desired compound.

Precursors SrCO_3 , Bi_2O_3 , Nb_2O_5 , Er_2O_3 , and Yb_2O_3 were weighed using weighing balance according to the stoichiometric calculation, and then a series of $\text{SrBi}_{2-x-y}\text{Nb}_2\text{Er}_x\text{Yb}_y\text{O}_9$ (SBN) ferroelectric ceramic ($x = 0.03$, $y = 0.01, 0.03, 0.06, 0.09$, and 0.12) is obtained. The naming of the samples prepared is shown in Table 1. The powder was hand grinded for 5 hours using a mortar pestle and then calcined at 950°C for 3 hours.



Fig.5-Steps to synthesize SBN

Calcined powder was again hand-grinded while mixing PVA (Polyvinyl chloride). The powder is now pelletized using a hydraulic press. Pellets of 10mm diameter were obtained and then sintered at 1050°C for 3hr. These sintered pellets are then used for different types of characterization i.e., XRD, SEM, FTIR, PL, UCL, and UV. The crystallographic structural analysis was studied under X-ray diffraction (XRD, Bruker D8 advanced X-ray diffractometer) using Cu-K α radiation ($\lambda=0.154\text{nm}$). The XRD spectrum for sintered $\text{SrBi}_{2-x-y}\text{Nb}_2\text{Er}_x\text{Yb}_y\text{O}_9$ ceramics was observed for the 2θ range 10° - 90° . SEM. Further, to analyze the vibrational wave bands, Fourier transform infrared spectroscopy (FTIR) was performed on the SBN fine powder using the PerkinElmer spectrum-II instrument. The PL excitation and emission spectra were measured using a JASCO FP- 8300 PC-Spectro fluorophotometer equipped with a xenon lamp, at an excitation wavelength of 488nm. The UCL spectra under the excitation of 980nm laser to understand the upconversion mechanism of Er^{3+} , Yb^{3+} co-doped SBN is obtained. Pump power dependence on UCL emission intensity is also studied along with the time decay analysis of SBN composition.

Table 1: Chemical composition and their respective sample code for the series of $\text{SrBi}_{2-x-y}\text{Nb}_2\text{Er}_x\text{Yb}_y\text{O}_9$ (SBN)

S.No.	COMPOSITION	SAMPLE CODE	Er(x)	Yb(y)
1	$\text{SrBi}_2\text{Nb}_2\text{O}_9$	SBE0Y0	0	0
2	$\text{SrBi}_{1.97}\text{Nb}_2\text{Er}_{0.03}\text{O}_9$	SBE3Y0	0.03	0
3	$\text{SrBi}_{1.96}\text{Nb}_2\text{Er}_{0.03}\text{Yb}_{0.01}\text{O}_9$	SBE3Y1	0.03	0.01
4	$\text{SrBi}_{1.94}\text{Nb}_2\text{Er}_{0.03}\text{Yb}_{0.03}\text{O}_9$	SBE3Y3	0.03	0.03
5	$\text{SrBi}_{1.91}\text{Nb}_2\text{Er}_{0.03}\text{Yb}_{0.06}\text{O}_9$	SBE3Y6	0.03	0.06
6	$\text{SrBi}_{1.88}\text{Nb}_2\text{Er}_{0.03}\text{Yb}_{0.09}\text{O}_9$	SBE3Y9	0.03	0.09
7	$\text{SrBi}_{1.85}\text{Nb}_2\text{Er}_{0.03}\text{Yb}_{0.12}\text{O}_9$	SBE3Y12	0.03	0.12

CHAPTER -4: CHARACTERIZATION TECHNIQUES

4.1 STRUCTURAL CHARACTERIZATION- XRD

There are various structural characterization techniques available. Some of the most widely used spectroscopies are X-ray diffraction (XRD), Transmission Electron Microscopy (TEM), Scanned electron microscopy (SEM), and neutron magnetic resonance (NMR) spectroscopy.

Here we study XRD for structural analysis, i.e., the crystallite nature of the synthesized material, which includes the degree of crystallinity, phase identification, lattice characteristics, and grain size. The X-ray powder diffraction method follows Bragg's law to analyze the crystal's nature. The following expression gives it:

$$2d \sin \theta = n\lambda$$

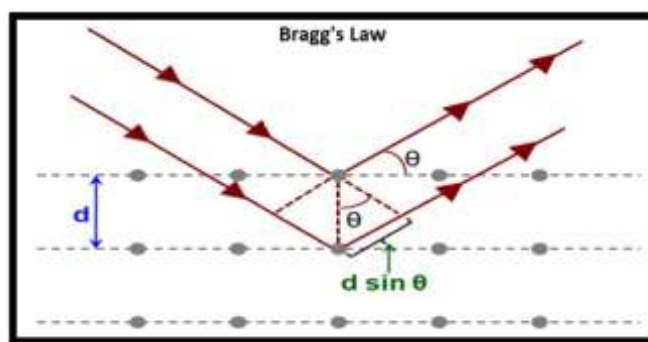


Fig.6-Bragg's law

The mechanism of X-ray diffraction is such that the X-ray targets the inner electrons of an atom. After interacting with the inner electrons, the scattered X-ray interacts within the vicinity of the atom. The interaction results give detailed information about the periodicity of atom arrangement in the material. The scattered X-rays constructively or destructively interfere with each other. The Bragg's law mathematically expresses constructive interference. The X-ray graph shows high peaks for constructive interference implying a high intensity of scattered X-rays. Using the Bragg's law, the interplanar spacing 'd' is calculated for each peak at a particular angle. Each peak observed in the X-ray pattern represents a specific Miller index. Each compound's unique X-ray pattern is available for scientific purposes. The powder diffraction file (PDF) contains x-ray patterns of all the possible compounds. For research motives, the JCPDF file for a specific compound is downloaded, and the X-ray results are matched to confirm the purity of phase formation. Bruker Diffractometer was used to obtain results for our sample.



Fig.7-Bruker D8 diffractometer

4.2 STRUCTURAL CHARACTERIZATION-SEM

A technique that is frequently used for structural characterization is scanning electron microscopy or SEM. A sample must be subjected to a high-energy electron beam for it to function. These electrons interact with the sample to produce a variety of signals that can be analyzed to determine the composition, crystallography, and surface morphology of the sample. SEM can reveal the following about the material:

- ✓ Surface Morphology: SEM excels at providing high-resolution images of a sample's surface, revealing details like:
 - Size and shape of particles or features
 - Texture and roughness
 - Presence of defects like cracks, pores, or inclusions

- ✓ Composition: SEM can be used in conjunction with Energy Dispersive Spectroscopy (EDS) to identify the elemental composition of a sample's surface region.

SEM is a versatile tool used across various scientific disciplines for structural analysis. Fig. 8 shows the working of SEM. It's useful for Examining the microstructure of metals, polymers, ceramics, and composites to understand their properties and performance. It also helps in studying the morphology of cells, tissues, and microorganisms. It can be used for analyzing fracture surfaces, gunshot residue, and other evidence materials. In the Semiconductor industry, it's utilized for inspecting integrated circuits for defects [25,26].

In summary, SEM is a powerful technique for structural characterization, providing valuable insights into a sample's surface morphology, composition, and other structural features.



Fig.8-Scanning Electron Microscopy (SEM)

4.3 CHEMICAL CHARACTERIZATION-FTIR

Fourier transform infrared (FTIR) analytical technique identifies the chemical structure of organic and inorganic materials. FTIR analysis is based on the wavelength of infrared radiations absorbed by a material. Only radiations with specific frequencies are absorbed by a material; it depends on the molecular bonds as different molecular bonds vibrate at different frequencies. In the FTIR spectra, the wavelengths absorbed are indicated as dips. The FTIR spectra of each material are unique, just like DNA or fingerprints. So, its analysis gives us quite detailed information about the different molecular bonds present in the material. FTIR spectroscopy is more beneficial than other infrared spectroscopies as it is faster and more precise and does not harm the sample [25-27].



Fig.9-PerkinElmer Spectrum FTIR spectrometer

4.4 OPTICAL CHARACTERIZATION-PL, UCL

There are various optical characterization techniques. Optical characterization is used to measure photoluminescence, luminescent lifetime, etc. This research analyses visible down-conversion photoluminescence, upconversion luminescence, pump power dependency on UCL emission intensity, and time decay.

Photoluminescence spectroscopy is an optical method to analyze the electronic configuration of a material. Fundamentally, optical characterization uses light to investigate a material's physical and chemical properties. Photoluminescence relies on photoexcitation, in which the material, when irradiated with a laser beam, causes the electrons to get excited and emit photons when relaxing back to the ground state via characteristic radiative and non-radiative phenomena. This excitation spectrum is particular to the energy difference between the ground and the excited states. Hence, beneficial to understand the properties of the material being characterized. Photoluminescence spectroscopy analyzes the phosphorescence and fluorescence, which in turn can be used to study the optoelectronic properties of many semiconductors, ceramics, and phosphors [25-28].

Upconversion luminescence (UCL) is the luminescence in which higher energy photons are emitted. It implies that more than one photon is absorbed to emit one photon. The energy of more than one incident photon combines to emit higher energy photons. This Upconversion emission is also called anti-stokes emission, as the lower wavelength photons are emitted during this process. The difference in energies of incident and emission photons is referred to as anti-stokes shift. The upconversion mechanism involves basic processes: GSA, ESA, ET, MPR, and radiative emission.



Fig.10-Up-conversion/ down-conversion Fluorescence spectroscopy

4.5 UV-VISIBLE SPECTROSCOPY



Fig.11-UV-Visible spectroscopy

UV-Vis DRS stands for Ultraviolet-Visible Diffuse Reflectance Spectroscopy. This method is used to examine a material's ability to absorb and reflect both visible and ultraviolet light. Following is an overview of the salient features:

- ✓ Ultraviolet-Visible (UV-Vis): This refers to the range of light being studied, encompassing both ultraviolet (shorter wavelengths) and visible (longer wavelengths) regions.
- ✓ Diffuse Reflectance: DRS focuses on light that is reflected by the material, as opposed to normal transmission spectroscopy, which measures light as it passes through a sample. This is especially helpful for examining materials that are hard to form thin films of, including powders, rough surfaces, or other materials.

Through the measurement of light reflection at various wavelengths, DRS offers data about:

- ✓ Electronic band structure: The energy needed by the material's electrons transition between different energy levels may be seen in the DRS spectrum. This aids in the determination of characteristics such as band gap, which is essential for comprehending conductivity and possible uses in photocatalysis or solar cells[22,23].
- ✓ Existence of specific elements or compounds: Certain elements or functional groups inside a material may be characterized by particular absorption properties in the UV-Vis range.

CHAPTER - 5: EXPERIMENTAL RESULTS

5.1 X-RAY DIFFRACTION(XRD)

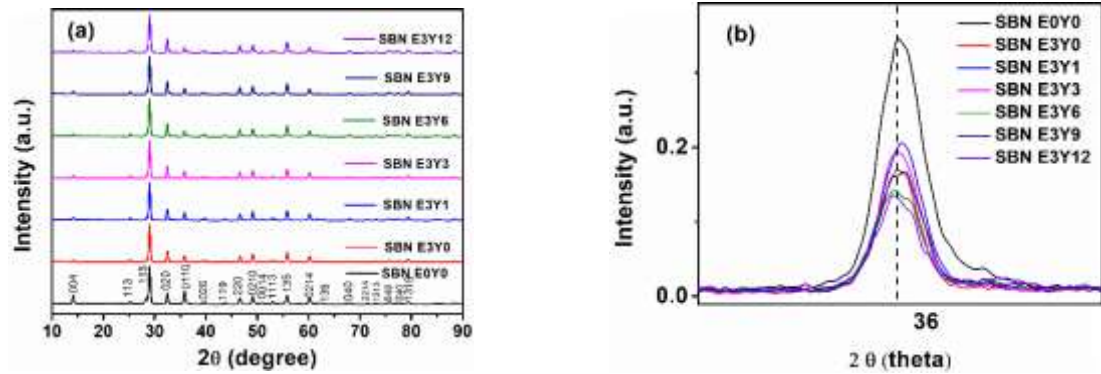


Fig.12-(a)XRD spectra for the series of SBN ferroelectric ceramics. (b)Shifting of the peak for various dopant concentrations.

Fig.12(a) illustrates the XRD pattern of pure phase SBN that underwent calcination at 950°C for 3 hours. The XRD peaks in the 2θ range from 10° to 80° show a good agreement with the standard JCPDF 00-049-0607. The high solubility of the Er^{3+} and Yb^{3+} ions and their successful substitution in the synthesized SBN ceramic compositions can be seen by the absence of additional peaks in the XRD spectra. The Bragg reflections obtained confirm the single-phase SBN having orthorhombic geometry having a phase group of $A21am$. The concentration of Er^{3+} is kept constant (i.e., $x=0.03$) while the concentration of Yb^{3+} is varied (i.e., $y=0.01, 0.03, 0.06, 0.09,$ and 0.12). The highest intensity peak corresponds to (115) planes at an angle(2θ) of 29° . The highest intensity plane was observed at (115) for all different compositions of SBN, conceding the BLSF with $n = 2$. The results agree with the reports, which confirms that the strongest diffraction corresponds to $(112n + 1)$ reflection for BLSF compositions in the Aurivillius phase.

Table 2: Lattice parameters for all compositions of SBN ferroelectric ceramics.

Parameters	a (Å)	b(Å)	c (Å)	V (Å ³)	Orthorhombic distortion (b/a)
SBNE0Y0	5.505	5.513	25.0350	759.871	1.0015
SBNE3Y0	5.513	5.520	25.0400	762.011	1.0012
SBNE3Y1	5.515	5.525	25.0406	762.996	1.0018
SBNE3Y3	5.510	5.535	25.0500	763.971	1.0045
SBNE3Y6	5.503	5.542	25.0650	764.422	1.0070
SBNE3Y9	5.507	5.543	25.0481	764.712	1.0065
SBNE3Y12	5.503	5.542	25.0650	764.422	1.0070

Fig. 12(b) shows the XRD pattern at the 2θ range of $28.2^\circ\sim 29.8^\circ$. The observed shift in the highest peak (115) of all specimens is quite inconspicuous with the rise in content of Yb^{3+} , indicating no evident changes in the crystalline cell volume(V), as can be confirmed in Table 2. This phenomenon is due to the similar ionic radii and the same electrical valence of Bi^{3+} (1.17\AA , C.No.=8), Er^{3+} (1.004\AA , C.No.=8), and Yb^{3+} (0.985\AA , C.No.=8). The lattice parameters are calculated using PowderX software and are tabulated in Table 2. Evaluation of lattice parameters from XRD shows the increase in orthorhombic distortion i.e., b/a value as the concentration of Yb^{3+} increases. The lattice parameters and unit cell volume increase as the content of Yb^{3+} rises.

5.2 SCANNING ELECTRON MICROSCOPE(SEM)

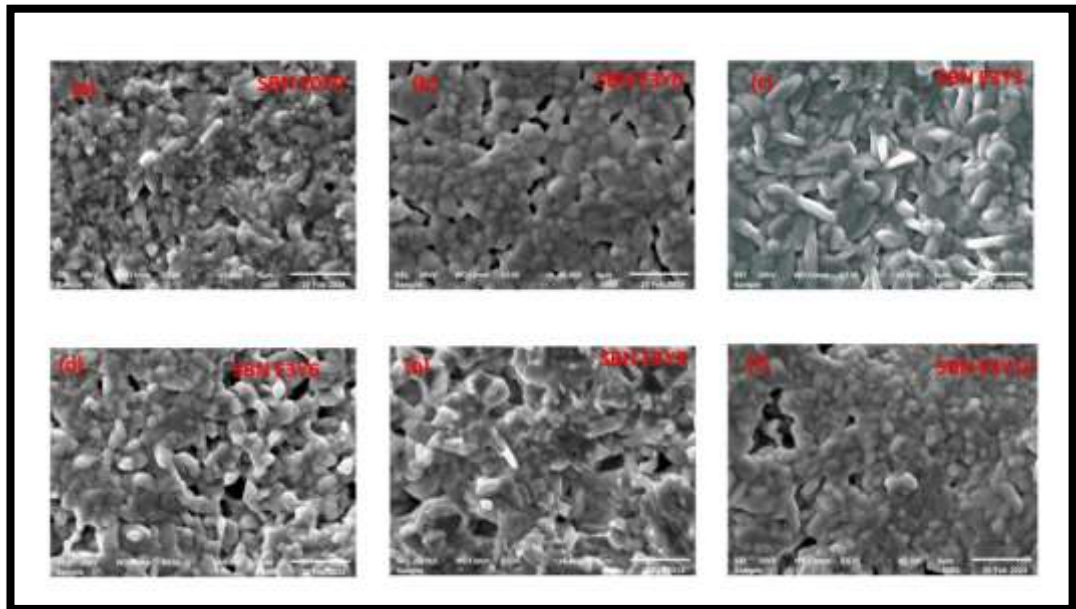


Fig.13-SEM analysis of a series of SBN ferroelectric ceramics.

From the analysis of SEM micrographs in Fig.13, it has been observed that the SBN ceramic has a randomly oriented plate-like structure, which is the typical characteristic of BLSF material. The average particle sizes are calculated using histograms (as in Fig.14) and are from $1.13\mu\text{m}$ for SBNE0Y0 to $2.23\mu\text{m}$ for SBNE3Y3. There's a slight increase in grain size for Yb^{3+} increases up to $y = 0.03$. Then the grain size decreases with an increase in Yb^{3+} concentration i.e., up to $0.936\mu\text{m}$ for SBNE3Y12. That's because the addition of a low concentration of Yb^{3+} leads to lattice distortion leading to the mass transfer and sintering process, thus grain size increases. When Yb^{3+} exceeds $y = 0.03$, the internal lattice structure is disrupted, ascribed to the stochastic distribution of Bi^{3+} and $(\text{Er}, \text{Yb})^{3+}$ in the lattice resulting in a slight reduction of grain size.

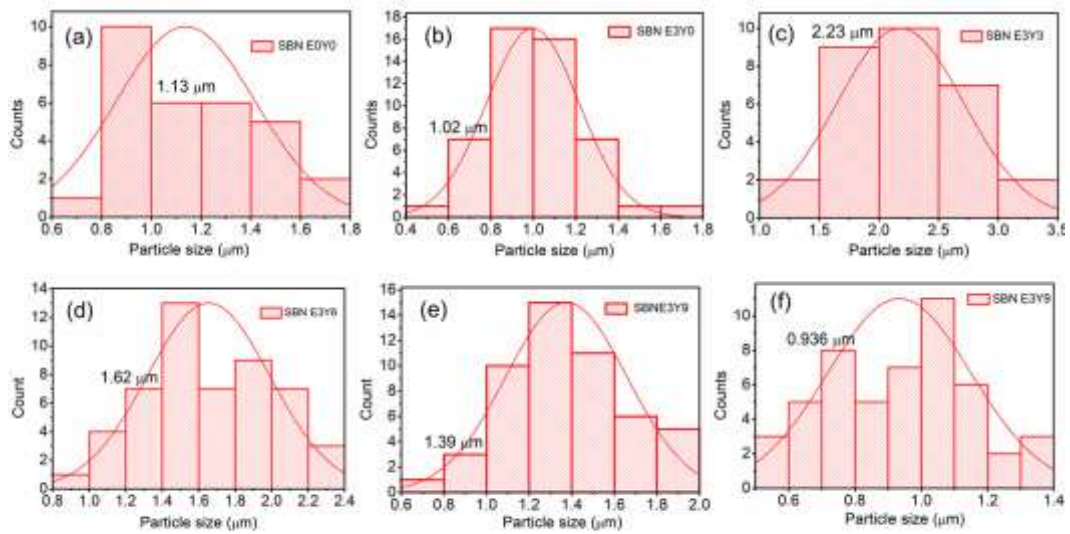


Fig.14-SEM histograms of series of SBN ferroelectric ceramic.

5.3 FOURIER TRANSFORM INFRARED (FTIR) SPECTROSCOPY

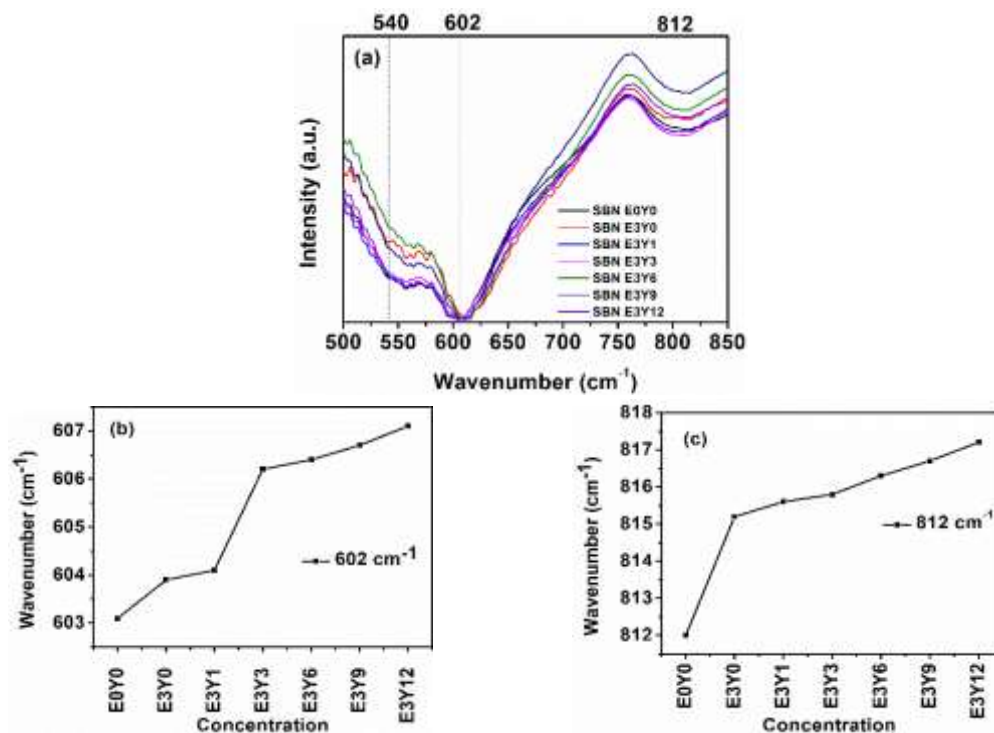


Fig.15-(a) FTIR spectra for the series of SBN ferroelectric ceramic, (b) FTIR band as the function of dopant concentration for wavenumber 602cm^{-1} , (c) FTIR band as the function of dopant concentration for wavenumber 812cm^{-1}

The FTIR spectra of prepared Er^{3+} and Yb^{3+} co-doped series of SBN ferroelectric ceramics are plotted in the above Fig.15(a). FTIR spectra show vibrational bands around 540cm^{-1} , 602cm^{-1} , and 812cm^{-1} demonstrating the stretching of the NbO_6 bond strongly which typically depends on the dopant concentration. The compositional dependence of dopant concentrations on FTIR is shown in Fig.15(b) and Fig.15(c). It is observed that the FTIR bands are affected by the dopant insertion resulting in the stretching of the NbO_6 bond [5-10].

5.4 PHOTOLUMINESCENCE(PL)

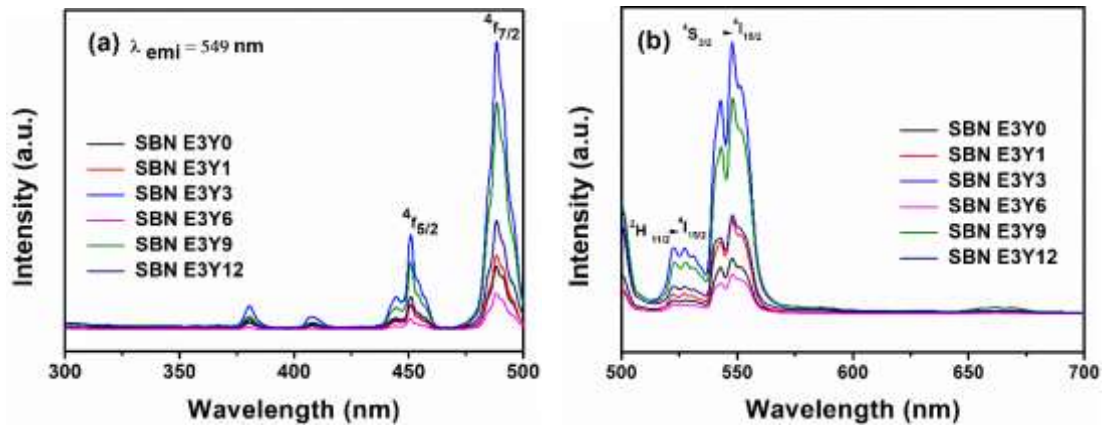


Fig.16-(a) Excitation spectra, (b) Emission spectra for the series of SBN ferroelectric ceramic

The excitation and emission PL spectra for the series of Er^{3+} , and Yb^{3+} co-doped SBN ferroelectric are represented in Fig. 16(a) and Fig.16(b), respectively. The excitation spectra are obtained at the emission wavelength of 549nm with maximum excitation obtained at 488nm. Emission spectra are obtained at the excitation wavelength of 488nm, with two strong green emission bands at 524nm and 549nm showing ${}^2\text{H}_{11/2}$ to ${}^4\text{I}_{15/2}$ and ${}^4\text{S}_{3/2}$ to ${}^4\text{I}_{15/2}$ transitions, respectively while there's one weak red emission band at 660nm wavelength are observed. Moreover, the Stark effect is responsible for the splitting of PL spectra into many components within the 540nm–549nm range. Initially, The PL intensity rises with increasing Yb^{3+} concentration up to $y= 0.03$, after which it falls due to concentration quenching, although the positions of the emission peaks for all stay unchanged. It occurs when the distance between dopant ions becomes so small that they can easily transfer their energy to each other, resulting in non-radiative radiations. Therefore, the Er^{3+} and Yb^{3+} co-doped SBN ceramics can be used as green light phosphors in photonic devices [11-16].

5.5 UP CONVERSION LUMINESCENCE (UCL)

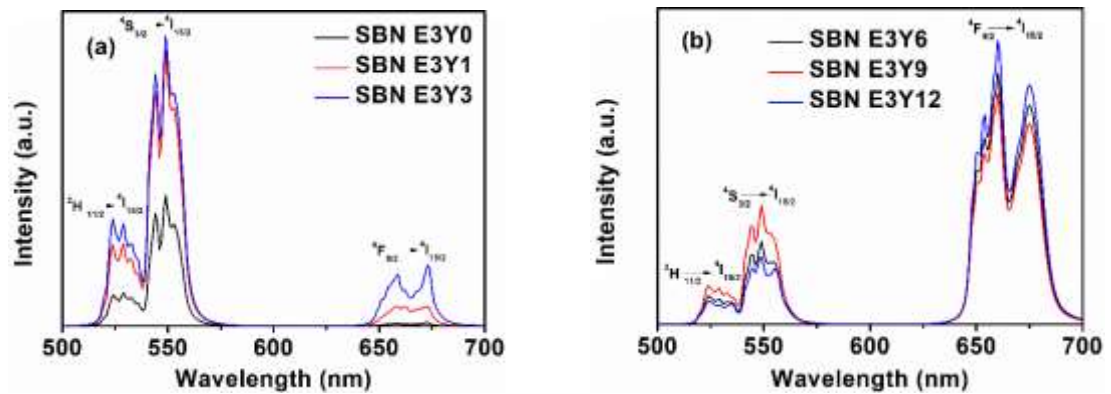


Fig.17-UCL spectra of the series of SBN ferroelectric ceramics.

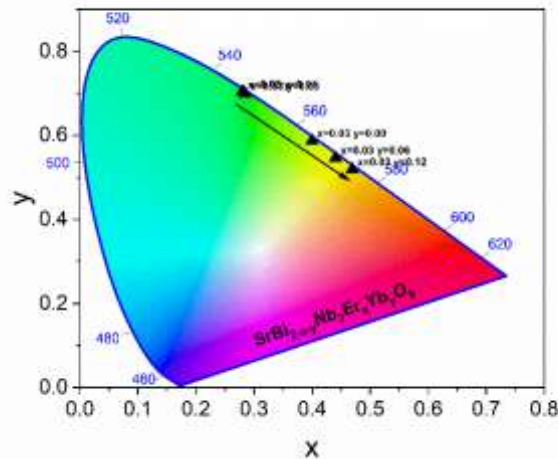


Fig.18-CIE plot of the series of SBN ferroelectric ceramics except SBNE0Y0

The UCL performance of Er^{3+} and Yb^{3+} co-doped SBN ceramics has been explored to achieve multifunctionality. Three absorption peaks have been observed in the range of 500nm –700 nm. The addition of Yb^{3+} ions leads to a rise in the intensity of absorption peaks. The transitions from $^2\text{H}_{11/2}$ to $^4\text{I}_{15/2}$ and from $^4\text{S}_{3/2}$ to $^4\text{I}_{15/2}$ are responsible for the two green emissions bands at 524nm and 549nm, respectively. A weaker red emission peak at 660nm indicates that Er^{3+} ions are transitioning from level $^4\text{F}_{9/2}$ to $^4\text{I}_{15/2}$. Two partial bands at 660nm and 670nm are observed in Fig.17 that are due to the $^4\text{F}_{9/2}$ energy level's crystal field splitting due to UCL. Till SBNE3Y3, green band intensity dominates however, when the Yb^{3+} concentration further rises, the red band begins to predominate due to concentration quenching. This suggests that multiple routes have been taken to fill energy levels. As the dopant concentration increases the distance between dopant ions decreases leading to effortless energy transfer and they begin to contribute to non-radiative transitions. The PL intensity decreases by the radiative transitions. It is observed from Fig.18 that as the concentration in Yb^{3+} is increased, there's an increase in the intensity of the red band (660 nm) by more than 10 times at SBNE3Y12 and that of the green band (549nm) more than 2.5 times whereas the

enhancement of the UC intensity is not on par with other doping concentrations. Due to CR in the phosphors, the green band's intensity, which was highest in SBNE3Y3 gradually reduces with an increase in the concentration of Yb^{3+} . This is due to the lattice phonon quenching process, which contributes to the gradual increase in the red band (660nm) intensity. This might be due to the increased degree of lattice distortion that ensued due to the optimum dopant concentration of Yb^{3+} .

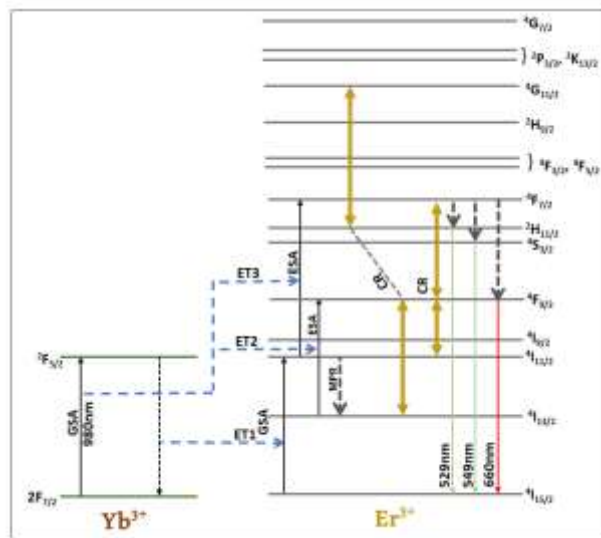


Fig.19-Energy transfer pathways between Yb^{3+} - Er^{3+} ions under 980 nm excitation

Green and red emissions both are generated from two-photon processes. Fig.19 shows the UC mechanism where there is perfect resonance between the $2F_{7/2}$ to $2F_{5/2}$ transition of Yb^{3+} and the $4I_{15/2}$ to $4I_{11/2}$ transition of Er^{3+} offering efficient energy transfer from Yb^{3+} to Er^{3+} . Upon 980nm laser irradiation, Yb^{3+} absorbs NIR photons which leads to the $2F_{7/2}$ to $2F_{5/2}$ upward transitions which resonantly donates the energy to the adjacent Er^{3+} , with Yb^{3+} falling back to its $2F_{7/2}$ ground state. Due to multi-phonon relaxation (MPR), certain Er^{3+} ions that are still at the $4I_{11/2}$ energy level eventually decay to the long-lived $4I_{13/2}$ energy level promoting the Er^{3+} ions to their excited state i.e., $4I_{15/2}$ to $4I_{11/2}$. Via energy level matching, the Er^{3+} ions can be populated to their higher excited states through resonant energy transfer from the sensitizers i.e., $4I_{11/2}$ to $4F_{7/2}$ or $4I_{13/2}$ to $4F_{9/2}$. The excited Er^{3+} ions then non-radiatively relax to the $2H_{11/2}$ and $4S_{3/2}$ states. As the electrons return to their ground state two green emissions corresponding to 524nm and 549nm are produced. Alternatively, the $4F_{9/2}$ state is non-radiatively populated from higher energy levels transfer from $4I_{13/2}$, which after some time results in red emissions centered at 660nm via the $4F_{9/2}$ to $4I_{15/2}$ transition. The smaller radius Er^{3+} , Yb^{3+} substitution for Bi^{3+} leads the crystal field's symmetry to weaken, which enhances the intensity of luminescence. The CR in the UCL process is why the red UC emission intensities are greater than the green ones when Yb^{3+} concentration increases above $y=0.03$ for the SBN ferroelectric ceramics [22-26].

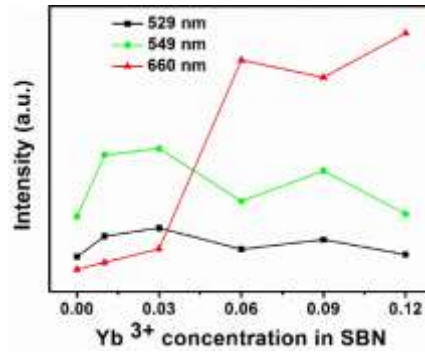


Fig.20- Enhancement in the green and red emission band intensities as the function of Yb³⁺ content.

Since beyond quenching concentration (SBNE3Y3), the interatomic distance gradually reduces, which results in non-radiative transitions. This results in the reduction of UCL intensity as multipole-multipole has greater probability over the electric multipole interaction. Further, the activator and sensitizer have an important role in deciding the critical Radius (R_C), which is calculated by the given formula:

$$R_C \approx 2 \left[\frac{3V}{4\pi X_C Z} \right]^{\frac{1}{3}}$$

Where Z is the number of host cations in the unit cell, V is unit-cell volume, and X_C is dopant concentration given by $X_C = (x+y)$, x and y are Er³⁺ and Yb³⁺ concentrations respectively. It is observed that for $X_C = 0.06$ ($x=0.03$, $y=0.03$), the critical distance in the presence of Yb³⁺ ion is $\sim 18.25\text{\AA}$, which is smaller than the critical radius calculated in the absence of the Yb³⁺ sensitizer ion which is $\sim 23.00\text{\AA}$. When critical distance, R_C in the presence of Yb³⁺ ion is smaller than the value obtained in the absence of Yb³⁺ ion efficiency of energy transfer increases as it occurs from the sensitizer Yb³⁺ to the activator Er³⁺ for the optimum concentration of the dopants i.e., $X_C = 0.06$ ($x=0.03$, $y=0.03$). Generally, when the critical distance value is less than 5\AA , exchange interaction plays a key role in concentration quenching. Meanwhile, if the critical distance is larger than 5\AA , then electric multipole interaction is observed to be predominant [27-30]. From the values obtained, it is inferred that multipole interaction is accountable for the quenching mechanism here.

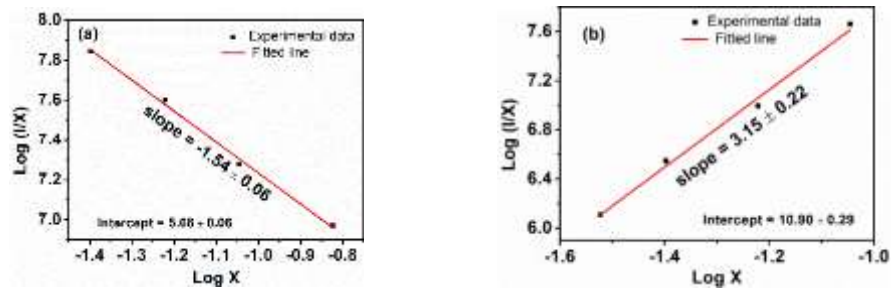


Fig.21-(a) Dexter plot of $\log(I/X)$ versus $\log(X)$ for 549 nm (b) Dexter plot of $\log(I/X)$ versus $\log(X)$ for 660 nm

For further understanding, based on Dexter's theory of sensitized luminescence in solids, S (fitting parameter) was calculated from Dexter's energy transfer formula given by:

$$\log \left[\frac{I}{X} \right] = b - \left[\frac{S}{3} \right] \log(X)$$

Where I denotes the UC intensity, X=(x+y) is the quenching concentration with x, and y are the Er³⁺ and Yb³⁺ concentrations respectively, and S is the fitting parameter with values 6,8,10 for dipole-dipole, dipole-quadrupole, quadrupole-quadrupole interactions respectively. To determine the S the slope of log(I/X) versus log(X) is obtained. For the emission at 549nm, the S value calculated is ~ 6, which indicates that the concentration quenching is due to dipole-dipole interaction, and for the emission at 660nm, the S value calculated is approximately 10 which corresponds to quadrupole-quadrupole interaction [10,11].

5.6 INFLUENCE OF PUMP POWER ON UCL

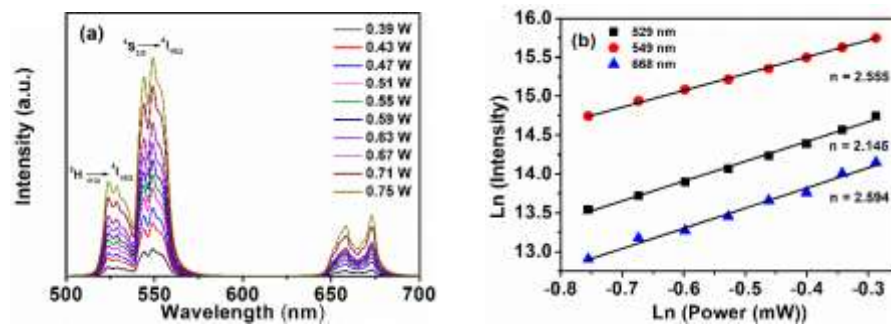


Fig.22-(a) Pump power dependency on UCL intensity of SBNE3Y3 ferroelectric ceramic (b) Log plot of pump power and UC intensity

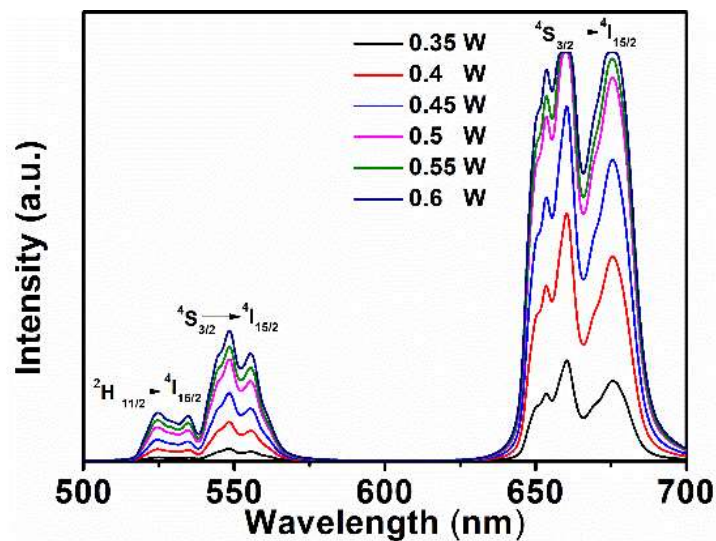


Fig.23-Pump power dependency on UCL intensity of SBNE3Y12 ferroelectric ceramic.

The compositions SBNE3Y3 and SBNE3Y12 were studied for the transitions from $^2H_{11/2}$, $^4S_{3/2}$, and $^4F_{9/2}$ to the ground state $^4I_{15/2}$ using various pump powers for a better understanding of the UCL mechanism. The pump power ranges for SBNE3Y3, and SBNE3Y12 are 0.39W to 0.75W and 0.35W to 0.60W, respectively. When pump power increases the UCL intensity improves in all upconverted emission bands. The relationship between intensity and pump power is given by:

$$I_{UCL} \propto P^n$$

Where I_{UCL} is the UCL intensity, n is the number of low-energy photons required in upconversion emissions, and P is for the excitation pump power. The log intensity-log excitation pump power is displayed in Fig.22(b). For both green (524nm and 549nm) and red (660nm) emissions of SBNE3Y3, the slope of the logarithmic plot gives n , which equals 2.55, 2.14, and 2.59, respectively [30-34]. In our work, an increased energy photon of wavelengths of 524nm, 549nm, and 660nm is produced by two less-energy photons that emit the green and red UC emission bands. The deviance in the n values for both the green and red emissions is approximated to the theoretical value of 2 because of the contribution of various mechanisms (ET, ESA, and non-radiative transitions) in the upconverted emission bands. Two photons are involved in the emission process as per the Pump power analysis done.

5.7 TIME DECAY ANALYSIS

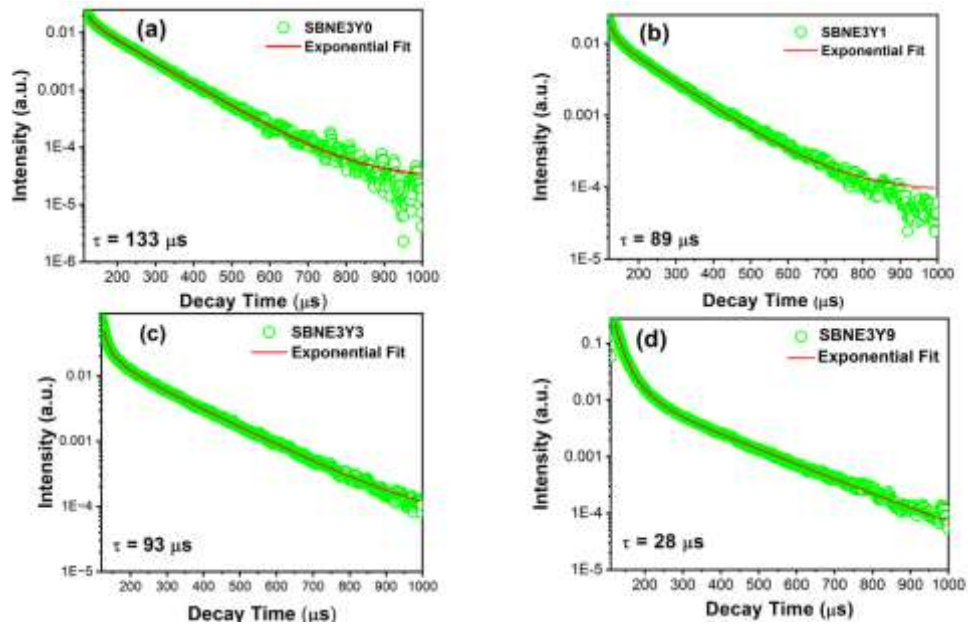


Fig.24-Time decay plots of all compositions of SBN ferroelectric ceramic at 549nm

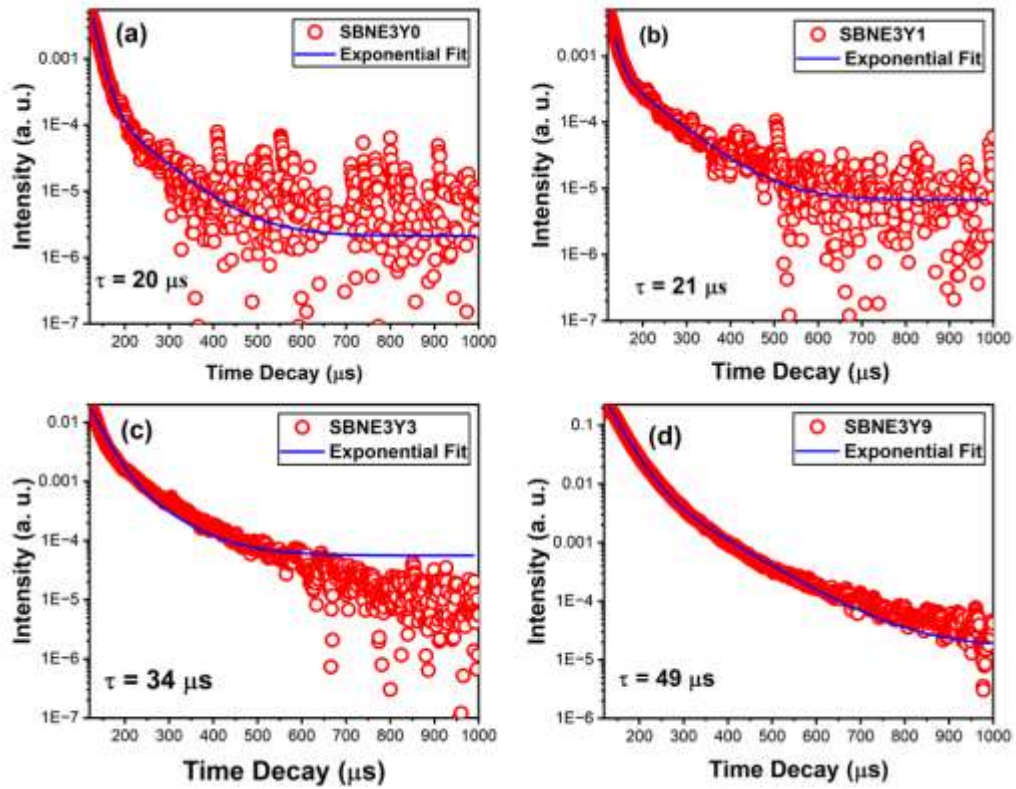


Fig.25-Time decay plots of all compositions of SBN ferroelectric ceramic at 660nm

The lifetime decay measurements were performed and studied for 549nm green emission and 660nm red emission for all compositions of SBN ceramic under 980nm excitation wavelength of pulsed type laser. The time-resolved photoluminescence (TRPL) decay was carried out to analyze radiative and non-radiative decay processes. Fluorescence decay transients of SBNE3Y0, SBNE3Y1, SBNE3Y3, and SBNE3Y9 at 549nm i.e., $^4S_{3/2} \rightarrow ^4I_{15/2}$ transition and 660nm i.e., $^4F_{9/2} \rightarrow ^4I_{15/2}$ are shown in Fig.24 and Fig.25, respectively when stimulated with a Xenon pulsed laser at 980nm. The curves were fitted by a single exponential decay function as given below:

$$I(t) = I_0 + Ae^{(-t/\tau)}$$

Here, $I(t)$ represent the time variation of luminous intensity, I_0 is the intensity at $t=0$, A is the fitting parameter, and τ represents a component of time decay at time t . At room temperature, PL emission and UCL spectra were examined under the wavelengths 488nm and 980nm. In both emission spectra, green emission bands (524nm and 549nm) and red emission bands (660nm) were found. The time decay profile indicates an average lifetime of Er^{3+} ions is $70\mu s$ and for Yb^{3+} it is calculated to be $37\mu s$ [34-38].

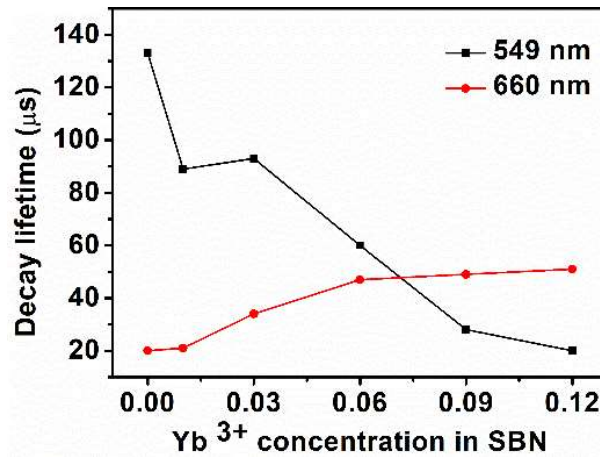


Fig.26- Variation of decay lifetime with Yb³⁺ concentration

From the analysis it is observed that the time decay values consistently decrease for the SBN ceramic at 549nm, starting from $t=133\mu s$ for SBNE3Y0 and to $t=28\mu s$ for SBNE3Y9. This suggests a decrease in non-radiative emission in the material. Time decay values at 660nm show increasing time decay values starting from $t=20\mu s$ for SBNE3Y0 and consistently increasing to $t=49\mu s$ for SBNE3Y9 suggesting an increase in radiative emission in the material. As the interatomic distance between the dopant ions reduces with increasing Yb³⁺ concentration, therefore the energy transfer is done more efficiently from Yb³⁺ to Er³⁺. Thus, the time decay when analyzed from a 549nm peak, the lifetimes are higher for the undoped SBN samples. Thus, the efficiency (η) of energy transfer (ET) in co-doped SBN ceramic can be calculated by:

$$\eta = 1 - \frac{\tau_a}{\tau_b}$$

Here, τ_a represents the mean lifetime for Er³⁺ and Yb³⁺ co-doped SBN ferroelectric ceramic, τ_b represents the lifetime of Er³⁺ doped SBN ferroelectric ceramic. The efficiency of the energy transfer process is enhanced by 51.8% by the incorporation of Yb³⁺ ions into the SBN host lattice [34-38].

Table 3: Fluorescence Time decay values for the series of SBN ferroelectric ceramic.

Sample name	524nm	549nm	660nm
SBNE3Y0	88 μs	133 μs	20 μs
SBNE3Y1	80 μs	89 μs	21 μs
SBNE3Y3	57 μs	93 μs	34 μs
SBNE3Y6	51 μs	60 μs	47 μs
SBNE3Y9	18 μs	28 μs	49 μs
SBNE3Y12	15 μs	20 μs	52 μs

5.8 UV-VISIBLE SPECTROSCOPY

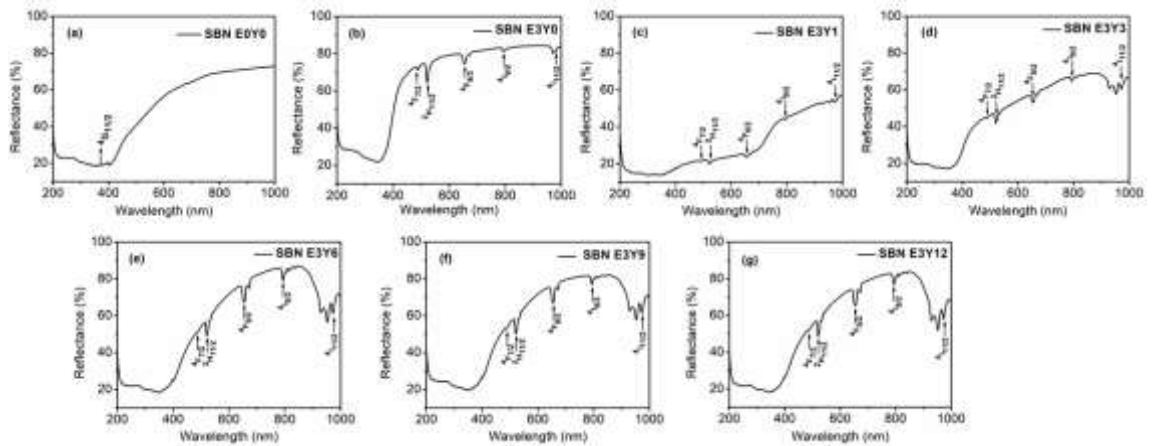


Fig.27-UV-visible spectra of all compositions of SBN ferroelectric ceramic.

UV-visible spectra of all compositions of SBN ferroelectric ceramic pellets were performed using a Perkin Elmer II Spectrometer. The onset of fundamental absorption edge near 350nm was observed in the reflectance spectra of all prepared thin films and is found to agree with the reported value. All samples exhibited interference fringe patterns with an average reflectance $> 70\%$ except SBNE3Y1, which implies good optical quality with a little scattering and internal absorption. Due to the high reflectance, SBN is a promising material in optoelectronic material applications. Meanwhile, the increase in reflectance is attributed to a higher refractive index value of SBN. For SBNE3Y1, the reflectance reduces significantly as the amount of scattering is higher compared to other samples [36-41].

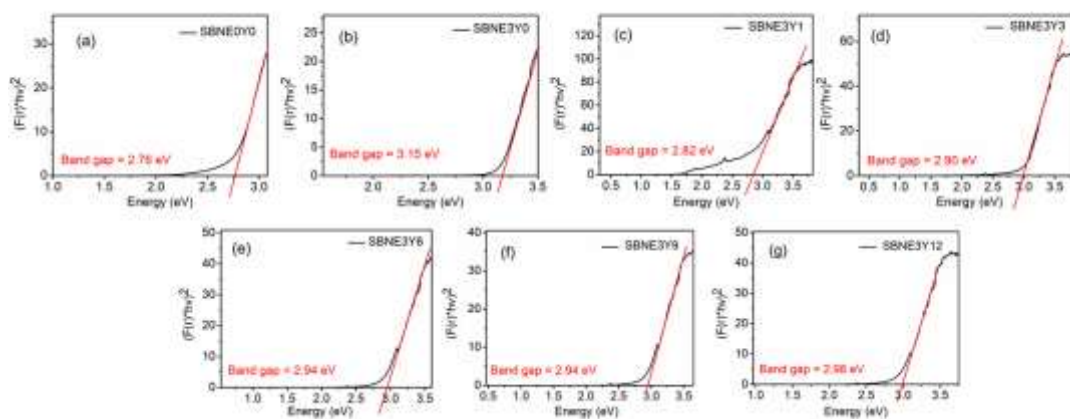


Fig.28-Tauc Plots of all compositions of SBN ferroelectric ceramic represented with their respective bandgaps.

The UV-visible spectra of all compositions of SBN were performed by the DRS method represented in Fig.-27. Their corresponding bandgaps were calculated by the Kubelka-Munk Function as given below.

$$F(R) = \frac{K}{S}$$

$$\text{Here, } K=(1-R)^2, S=2R$$

Here K is the molar absorption coefficient, S is the scattering factor, and R is the reflectance of the material, which is calculated by the formula given,

$$R = \frac{R(\%)}{100}$$

The band gaps calculated for the respective samples are represented in Fig.28. The values of bandgap were obtained by extrapolating the linear part of $(F(R)*hv)^2$ versus $hv(\text{energy})$ plot as shown in Fig.28(a-g). According to the observations, Bandgaps increase with higher doping concentration in the ferroelectric ceramic samples. The x-axis is Energy in terms of hv , whereas the y-axis is plotted in terms of $(F(R)*hv)^n$, where n value is 2 as direct bandgap and for indirect bandgap, n is $\frac{1}{2}$ [36-39].

CHAPTER -6: RESULTS AND CONCLUSIONS

The ferroelectric ceramic for different compositions of $\text{SrBi}_{2-x-y}\text{Nb}_2\text{Er}_x\text{Yb}_y\text{O}_9$ ($x = 0.00, 0.03, y = 0.00, 0.01, 0.03, 0.06, 0.09, \text{ and } 0.12$) has been prepared using the solid-state method. The formation of pure phase $\text{SrBi}_2\text{Nb}_2\text{O}_9$ has been confirmed by XRD spectra corresponding to orthorhombic geometry having phase group $A21am$. The high solubility of the Er^{3+} and Yb^{3+} ions in synthesized SBN is confirmed by the absence of additional peaks in the XRD spectra. The highest intensity peak corresponds to (115) planes at an angle (2θ) of 29° , conceding the BLSF with $n = 2$. The observed shift in peak (115) of all specimens is quite inconspicuous with the rise in content of Yb^{3+} , indicating no evident changes in the crystalline cell volume (V). Evaluation of lattice parameters shows the increase in orthorhombic distortion i.e., b/a value as the concentration of Yb^{3+} increases. The lattice parameters and unit cell volume increase as the content of Yb^{3+} rises. From the analysis of SEM micrographs, the SBN ceramic has a randomly oriented plate-like structure. The average particle sizes range from $1.13\mu\text{m}$ for SBNE0Y0 to $2.23\mu\text{m}$ for SBNE3Y3 and then decrease to $0.936\mu\text{m}$ for SBNE3Y12 as the lattice structure gets disrupted above $y=0.03$. FTIR spectra show vibrational bands around 540cm^{-1} , 602cm^{-1} , and 812cm^{-1} justifying the characteristic bands of ferroelectric materials. The PL excitation spectra are obtained at the emission wavelength of 549nm with maximum excitation obtained at 488nm . Emission spectra are obtained at the excitation wavelength of 488nm , with two strong green emission bands at 524nm and 549nm corresponding to ${}^2\text{H}_{11/2}$ to ${}^4\text{I}_{15/2}$ and ${}^4\text{S}_{3/2}$ to ${}^4\text{I}_{15/2}$ transitions, respectively while there is one weak red emission band at 660nm wavelength. The PL intensity rises with increasing Yb^{3+} concentration up to $y=0.03$, after which it falls due to concentration quenching as the distance between dopant ions becomes so small that they can easily transfer their energy to each other, resulting in non-radiative radiations. The UCL spectra excited by 980nm laser reveal that the addition of Yb^{3+} ions leads to a rise in the intensity of absorption peaks, showing two UCL bands at 524nm and 549nm in the green region and a single red band at 660nm . The green band dominates up to configuration SBNE3Y3 after which red emission dominates as the concentration of Yb^{3+} increases as the distance between dopant ions decreases leading to multiple pathways for energy transfer. The compositions SBNE3Y3 and SBNE3Y12 were studied for the transitions from ${}^2\text{H}_{11/2}$, ${}^4\text{S}_{3/2}$, and ${}^4\text{F}_{9/2}$ to the ground state ${}^4\text{I}_{15/2}$ using various pump powers for a better understanding of the UCL mechanism. When pump power increases the UCL intensity improves in all upconverted emission bands. Pump power dependence on UCL emission intensity shows that the two photons contribute to green and red UC emissions. The time decay analysis of SBN composition showed that the average decay time of Er^{3+} is $70\mu\text{s}$ and that of Yb^{3+} is $37\mu\text{s}$. The efficiency of the energy transfer process is enhanced by 51.8% by the incorporation of Yb^{3+} ions into the SBN host lattice. The DRS revealed the band gaps of the SBN ranging from values 2.7eV to 3.1eV . All the findings suggest that SBN can be considered for achieving multifunctionality. UCL studies suggest that $\text{Er}^{3+}/\text{Yb}^{3+}$ co-doped SBN can be used where tunability of green light into red light is required and the efficiency of energy transfer can be enhanced with the incorporation of Yb^{3+} as the luminescent center. Also, UV-visible studies reveal that the bandgaps increase with higher doping concentration.

REFERENCES

- [1] Z. Tianmin, Z. Yanqiu, W. Zhongli, and C. Baojiu, "Concentration effect and temperature quenching of upconversion luminescence in BaGd₂ZnO₅:Er³⁺/Yb³⁺ phosphor," *J. Rare Earth.*, vol. 33, no. 7, pp. 686, 2015, doi: 10.1016/S1002-0721(14)60471-3.
- [2] M. K. Mahata, T. Koppe, T. Mondal, C. B. Sewitz, K. Kumar, V. K. Rai, H. Hofsass, and U. Vetter, "Incorporation of Zn²⁺ ions into BaTiO₃:Er³⁺/Yb³⁺ nanophosphor: an effective way to enhance upconversion, defect luminescence, and temperature sensing," *Phys. Chem. Chem. Phys.*, vol. 17, pp. 20741-20753, 2015, doi: 10.1039/c5cp01874a.
- [3] A. Banwal, Ankita, and Renuka Bokolia. "Thermometric sensing performance in Erbium modified SrBi_{2-x}Nb₂Er_xO₉ ferroelectric ceramic for optoelectronic devices." *Ceramics International* 48, no. 23 (2022): 34405-34414.
- [4] A. Banwal & R. Bokolia, "Efficient tunable temperature sensitivity in thermally coupled levels of Er³⁺/Yb³⁺ co-doped BaBi₂Nb₂O₉ ferroelectric ceramic," *Journal of Luminescence*, 263,120071,2023.
- [5] A. Banwal & R. Bokolia, "Enhanced upconversion luminescence and optical temperature sensing performance in Er³⁺ doped BaBi₂Nb₂O₉ ferroelectric ceramic," *Ceramics International*, 42, 2230-2240, 2021.
- [6] M. Narwan, A. Banwal, R. Sharma, R. Bokolia, "Non-invasive thermal sensing and improved recoverable energy storage density of Bi_{0.5}Na_{0.5}TiO₃: Er³⁺ doped multifunctional ferroelectric ceramic," *J. Lumin.* 265(2):120236, 2024.
- [7] A. Banwal & R. Bokolia, "Preparation and characterisations of Yb³⁺ substituted BaBi_{2-y}Nb₂Yb_yO₉ ferroelectric ceramic," *Materials Today: Proceedings* 62 (5) 3782-3785, 2022.
- [8] A. Banwal & R. Bokolia, "Effect of Er³⁺ ion doping on structural, ferroelectric and up/down conversion luminescence in BaBi₂Nb₂O₉ ceramic," 47(03) 4692-4695, 2021.
- [9] A. Banwal & R. Bokolia, "Phase evolution and microstructure of BaBi₂Nb₂O₉ ferroelectric ceramics," *Materials Today: Proceedings* 46(4) 10121-10124, 2020.
- [10] Dexter DL (1953) A theory of sensitized luminescence in solids. *J Chem Phys* 21:836-850. <https://doi.org/10.1063/1.1699044>
- [11] Dexter DL, Schulman JH (1954) Theory of concentration quenching in inorganic phosphors. *J Chem Phys* 22:1063-1070. <https://doi.org/10.1063/1.1740265>
- [12] A. Shandilya, Ram Sagar Yadav, Ajai K. Gupta, and K. Sreenivas. "Temperature-dependent light upconversion and thermometric properties of Er³⁺/Yb³⁺-codoped SrMoO₄ sintered ceramics." *Journal of Materials Science* 56 (2021): 12716-12731.
- [13] Haonan Liu, Jiangting Wang, Hua Wang, Jiwen Xu, Changrong Zhou, Wei Qiua, "Er³⁺ and Sr(Bi_{0.5}Nb_{0.5})O₃ modified (K_{0.5}Na_{0.5})NbO₃: A new transparent fluorescent ferroelectric ceramic with high light transmittance and good luminescence performance," *Ceramic International*, 48, 4230-4237,2022.

- [14] T. Wei, T.B. Zhang, Y.J. Ma, Y.F. Xie, C.Z. Zhao, F.M. Yang, H.Y. Xiao, Y. Zhao, "Up-conversion photoluminescence and temperature sensing properties of Er³⁺-doped Bi₄Ti₃O₁₂ nanoparticles with good water-resistance performance," RSC Adv. 6 7643–7652, 2016.
- [15] P.Haro Gonzalez, I.R.Martin, L.L.Martin, D.Kowalska, J.M.Caceres. "Crystallization effect on Tm³⁺-Yb³⁺ codoped SBN glass ceramics," 32(10), 1385-1388, 2010.
- [16] X. Wu, C. Fang, J. Lin, C. Liu, L. Luo, M. Lin, X. Zheng, C. Lin, "Tetragonal Er³⁺ doped (K_{0.48}Na_{0.48}Li_{0.04}) (Nb_{0.96}Bi_{0.04})O₃: lead-free ferroelectric transparent ceramics with electrical and optical multifunctional performances. Ceramic International," 444908–4914, 2018.
- [17] Z. Liang, E. Sun, S. Pei, L. Li, F. Qin, Y. Zheng, H. Zhao, Z. Zhang, W. Cao, "Influence of phase transitions on green fluorescence intensity ratio in Er³⁺ doped K_{0.5}Na_{0.5}NbO₃ ceramic. Opt Express," 24 29209–29215, 2016.
- [18] A. Enachi, O. Toma, S. Georgescu, "Luminescent Er³⁺ centers in CaSc₂O₄:Er³⁺: Yb³⁺ upconversion phosphor, J. Lumin. 231117816, 2021.
- [19] R. Shaily & R. Bokolia, "Structural and photoluminescence properties of Er³⁺ doped SrBi₂Nb₂O₉ ceramics," Materials Today: Proceedings, 2214-7853,2021.
- [20] R. Bokolia, O.P. Thakur, V.K. Rai, S.K. Sharma, K. Sreenivas, "Dielectric, ferroelectric and photoluminescence properties of Er³⁺ doped Bi₄Ti₃O₁₂ ferroelectric ceramics," Ceramics International 41 x 6055–6066, 2015.
- [21] Y. Zhang, R. Chu, Z. Xu, S. Zhang, C. Zhang, G. Li, "Electrical and luminescence properties, and energy band structure of SrBi_{2-x}Er_xNb₂O₉ multifunctional ceramics," Ceram. Int. 4730938–30946, 2021.
- [22] Q. Wei, Z. Zhou, W. Zhang, G. Tang, Q. Liu, L. Qin, H. Shi, "Tunable electronic band structure, luminescence properties and thermostability of (Gd_{1-x}La_x)₂Si₂O₇: Ce scintillator by adjusting La/Gd ratio," J. Rare Earths 39657–665, 2021.
- [23] J. Lin, W. Jing, H.Wang, J. Xu, X.Wu, C. Lin, T. Lin, X. Zheng, L. Luo, "Emission colortunable and optical temperature sensing properties of Er³⁺/La³⁺ co-doped (K_{0.5}Na_{0.5})NbO₃ optoelectronic transparent ceramic," J. Lumin. 213 158–163, 2019.
- [24] X. Ye, Y. Luo, S. Liu, D. Hou, W. You, "Intense and color-tunable upconversion luminescence of Er³⁺ doped and Er³⁺/Yb³⁺ co-doped Ba₃Lu₄O₉ phosphors," J.Alloy. Compd. 701 806–815, 2017.
- [25] R.Bokolia, Manisha Mondal, V. K. Rai, and K. Sreenivas. "Enhanced infrared-to-visible up-conversion emission and temperature sensitivity in (Er³⁺, Yb³⁺, and W⁶⁺) tri-doped Bi₄Ti₃O₁₂ ferroelectric oxide." Journal of Applied Physics 121, no. 8 (2017).
- [26] R.Bokolia, O. P. Thakur, Vineet K. Rai, S. K. Sharma, and K. J. C. I. Sreenivas. "Dielectric, ferroelectric and photoluminescence properties of Er³⁺ doped Bi₄Ti₃O₁₂ ferroelectric ceramics." Ceramics International 41, no. 4 (2015): 6055-6066.

[27] R. Bokolia, O. P. Thakur, V. K. Rai, S. K. Sharma, and K. Sreenivas. "Electrical properties and light upconversion effects in $\text{Bi}_{3.79}\text{Er}_{0.03}\text{Yb}_{0.18}\text{Ti}_{3-x}\text{W}_x\text{O}_{12}$ ferroelectric ceramics." *Ceramics International* 42, no. 5 (2016): 5718-5730.

[28] Mojumdar, Pooja, Ritushree Shaily, and Renuka Bokolia. "Structural properties of strontium bismuth niobate ($\text{SrBi}_2\text{Nb}_2\text{O}_9$) ferroelectric ceramics." *Materials Today: Proceedings* 47 (2021): 4661-4665.

[29] Lojpur, Vesna, G. Nikolić, and M. D. Dramićanin. "Luminescence thermometry below room temperature via up-conversion emission of Y_2O_3 : Yb^{3+} , Er^{3+} nano phosphors." *Journal of Applied Physics* 115, no. 20 (2014).

[30] Cao, Qiufeng, Dengfeng Peng, Hua Zou, Jun Li, Xusheng Wang, and Xi Yao. "Up-conversion luminescence of Er^{3+} and Yb^{3+} co-doped $\text{CaBi}_2\text{Ta}_2\text{O}_9$ multifunctional ferroelectrics." *Journal of Advanced Dielectrics* 4, no. 03 (2014): 1450018.

[31] Ma, Chunlin, Weiping Zhou, Zhixing Gan, Xingyu Wang, Weishi Tan, Zhengming Zhang, and Zhangyin Zhai. "Upconversion photoluminescence modulation by electric field poling in Er^{3+} doped $(\text{Ba}_{0.85}\text{Ca}_{0.15})(\text{Zr}_{0.1}\text{Ti}_{0.9})\text{O}_3$ piezoelectric ceramics." *Journal of Alloys and Compounds* 794 (2019): 325-332.

[32] Yao, Zhongran, Ruiqing Chu, Zhijun Xu, Jigong Hao, Wei Li, and Guorong Li. "Processing and enhanced electrical properties of $\text{Sr}_{1-x}(\text{K}_{0.5}\text{Bi}_{0.5})_x\text{Bi}_2\text{Nb}_2\text{O}_9$ lead-free piezoelectric ceramics." *Ceramics International* 42, no. 9 (2016): 10619-10623.

[33] Soni, Abhishek Kumar, Astha Kumari, and Vineet Kumar Rai. "Optical investigation in shuttle like BaMoO_4 : Er^{3+} - Yb^{3+} phosphor in display and temperature sensing." *Sensors and Actuators B: Chemical* 216 (2015): 64-71.

[34] Mukhopadhyay, Lakshmi, Vineet Kumar Rai, Renuka Bokolia, and K. Sreenivas. "980 nm excited $\text{Er}^{3+}/\text{Yb}^{3+}/\text{Li}^+/\text{Ba}^{2+}$: NaZnPO_4 upconverting phosphors in optical thermometry." *Journal of Luminescence* 187 (2017): 368-377.

[35] Liu, Fang, Xiangping Jiang, Chao Chen, Xin Nie, Xiaokun Huang, Yunjing Chen, Hao Hu, and Chunyang Su. "Structural, electrical and photoluminescence properties of Er^{3+} -doped $\text{SrBi}_4\text{Ti}_4\text{O}_{15}$ - $\text{Bi}_4\text{Ti}_3\text{O}_{12}$ inter-growth ceramics." *Frontiers of Materials Science* 13 (2019): 99-106.

[36] Yu, Lei, Jigong Hao, Zhijun Xu, Wei Li, Ruiqing Chu, and Guorong Li. "Strong photoluminescence and good electrical properties in Eu-modified $\text{SrBi}_2\text{Nb}_2\text{O}_9$ multifunctional ceramics." *Ceramics International* 42, no. 13 (2016): 14849-14854.

[37] Du, Peng, Laihui Luo, Weiping Li, and Qingying Yue. "Upconversion emission in Er-doped and Er/Yb-codoped ferroelectric $\text{Na}_{0.5}\text{Bi}_{0.5}\text{TiO}_3$ and its temperature sensing application." *Journal of Applied Physics* 116, no. 1 (2014).

[38] Li, LianJie, Ye Tong, Jing Chen, YiHang Chen, Ghulam Abbas Ashraf, LiPing Chen, Tao Pang, and Hai Guo. "Up-conversion and temperature sensing properties of $\text{Na}_2\text{GdMg}_2(\text{VO}_4)_3$: Yb^{3+} , Er^{3+} phosphors." *Journal of the American Ceramic Society* 105, no. 1 (2022): 384-391.

[39] Liu, Yuan, Gongxun Bai, Er Pan, Youjie Hua, Liang Chen, and Shiqing Xu. "Upconversion fluorescence property of $\text{Er}^{3+}/\text{Yb}^{3+}$ codoped lanthanum titanate microcrystals for optical thermometry." *Journal of Alloys and Compounds* 822 (2020): 153449.

[40] Xing, Junhao, Fei Shang, and Guohua Chen. "Upconversion luminescence of $\text{Yb}^{3+}/\text{Er}^{3+}$ co-doped NaSrPO_4 glass ceramic for optical thermometry." *Ceramics International* 47, no. 6 (2021): 8330-8337.

[41] Wang, Yining, Mengmeng Shang, Shuai Huang, Yixin Sun, Yiyang Zhu, Xiaole Xing, Peipei Dang, and Jun Lin. "Continuous Ultra-Broadband Near-Infrared Sc_2O_3 -Based Nanophosphor Realized by Spectral Bridge of Cr^{3+} - Yb^{3+} - Cr^{4+} for Multiple Optical Applications." *Advanced Optical Materials* 11, no. 19 (2023): 2300517.

APPENDICES

PLAGIARISM REPORT

Similarity Report

PAPER NAME

THESIS plag.docx

WORD COUNT

9849 Words

CHARACTER COUNT

57012 Characters

PAGE COUNT

52 Pages

FILE SIZE

4.0MB

Renuka

SUBMISSION DATE

Jun 5, 2024 1:08 PM GMT+5:30

REPORT DATE

Jun 5, 2024 1:09 PM GMT+5:30

● 10% Overall Similarity

The combined total of all matches, including overlapping sources, for each database.

- 4% Internet database
- 8% Publications database
- Crossref database
- Crossref Posted Content database
- 2% Submitted Works database

● Excluded from Similarity Report

- Bibliographic material
- Quoted material
- Cited material
- Small Matches (Less than 12 words)

● 10% Overall Similarity

Top sources found in the following databases:

- 4% Internet database
- 8% Publications database
- Crossref database
- Crossref Posted Content database
- 2% Submitted Works database

TOP SOURCES

The sources with the highest number of matches within the submission. Overlapping sources will not be displayed.

1	Ankita Banwal, Renuka Bokolia. "Thermometric sensing performance i...	3%
	Crossref	
2	Wenfeng Wang, Jun Wang. "Investigation of microplastics in aquatic e...	2%
	Crossref	
3	Yuying Zhang, Yanliang Wei, Anqi Zhang, Ruiqing Chu, Guorong Li, Cha...	2%
	Crossref	
4	infona.pl	2%
	Internet	

Renuka

CONFERENCE REGISTRATION PROOF

ICAMNOP-2023 - Payment Acknowledgement ✉



ICAMNOP-2023 icamnop@dtu.ac.in [via sendgrid.net](mailto:icamnop@dtu.ac.in)
to me

Sat, Nov 25, 2023, 11:23AM ☆ 😊 ↶ ⋮

Dear Ms. SHOBHANGNA SINGH,

Your payment has been successfully received

ICAMNOP-2023

Thanks and Regards

Prof. Vinod Singh

Renuka

↶ Reply

↷ Forward



ICAMNOP 2023-Abstract status ✉



ICAMNOP 2023 DTU icamnop@dtu.ac.in
to me

Fri, Nov 30, 2023, 12:47PM ☆ 😊 ↶ ⋮

Dear Ms. SHOBHANGNA SINGH

Warm greetings from the ICAMNOP 2023 (International Conference on Atomic, Molecular, Material, Nano and Optical Physics with Applications)

We are pleased to inform you that your abstract **ABS46 "Structural, photoluminescence and ferroelectric behaviour of Er³⁺/Yb³⁺ co-doped SrBi₂Nb₂O₉ ferroelectric ceramic for multifunctional devices"** has been accepted for a **Poster** presentation at the ICAMNOP 2023 Conference.

We are thrilled to have you participate in this exciting conference, which is scheduled to take place in Delhi, India from 20th to 22nd December 2023. With an incredible lineup of technical presentations and discussions, we are confident that ICAMNOP 2023 will be a memorable and enriching experience, and you will benefit greatly from this platform.

The details for registration to the conference can be found at <https://icamnop.in/registration>. Please remember that Early Bird Registration ends on 30th November 2023.

We look forward to seeing you at ICAMNOP Conference

Warm Regards

Prof. Vinod Singh

Convener, ICAMNOP-2023 &

Professor, Department of Applied Physics

Delhi Technological University (DTU),

Shaheed Daultpur, Bawana Road, Delhi-110042, India

Email vinod.singh@dtu.ac.in; vinod@dtu.ac.in

Conference website: <https://www.icamnop.in/>

Conference Email: icamnop@dtu.ac.in

Renuka

CONFERENCE PARTICIPATION CERTIFICATE



CONFERENCE PAPER

Structural, photoluminescence, and ferroelectric behaviour of Er³⁺ / Yb³⁺ co-doped SrBi₂Nb₂O₉ ferroelectric ceramic for multifunctional devices

Shobhangna Singh^a, Abdul Basith^a, Ankita Banwal^a, Megha Narwan^a, Renuka Bokolia^{a*}
^aCFMRL, Department of Applied Physics, Delhi Technological University, Delhi, India-110042

Abstract: A series of SrBi_{2-x-y}Nb₂Er_xYb_yO₉ ferroelectric ceramics (x = 0.00, 0.03, y = 0.00, 0.01, 0.03, and 0.06) has been prepared by solid state method. The formation of pure phase SrBi₂Nb₂O₉ is confirmed by XRD spectra corresponding to orthorhombic geometry having phase group A21am. Microstructure of the ceramic resembles plate-like structures. The FTIR bands at 602 cm⁻¹ and 814 cm⁻¹ justified the characteristic bands of bismuth-layered structure ferroelectric (BLSF) materials. The PL spectra were obtained under the excitation of 488 nm. Two green PL emission bands were found at 525 and 549 nm and one weak red band at 660 nm. The highest PL intensity is found at x = 0.03, y = 0.03; after this concentration, the intensity degrades due to the concentration quenching effect. The PE loops showed decent shapes with the remnant polarization at 2.202 μC/cm² for (x = 0.03, y = 0.03) doped ceramics at an applied electric field of 30 kV/cm. Thus, the prepared ceramic can be used in multifunctional devices.

Keywords: SBN; XRD; FTIR; photoluminescence; ferroelectric; ceramics.

STATUS OF PAPER

